The Formation of a Cooling-induced Mesovortex in the Trailing Stratiform Region of a Midlatitude Squall Line

DA-LIN ZHANG

Department of Atmospheric and Oceanic Sciences, McGill University, Montreal, Quebec, Canada

(Manuscript received 2 December 1991, in final form 2 March 1992)

ABSTRACT

There have been some ambiguities in recent observational studies as to whether midlevel mesovortices are induced by latent heating or cooling, and develop in the descending or ascending portion of mesoscale convective systems (MCS's). In this study, a comprehensive examination of a cooling-induced mesovortex in the trailing stratiform region of a midlatitude squall line that occurred on 10–11 June 1985 during the Preliminary Regional Experiment for STORM-Central (PRE-STORM) is presented using a 20-h high-resolution simulation of the squall system.

This cooling-induced midlevel vortex originates from the preexisting cyclonic vorticity associated with a traveling meso-α-scale short wave. The vortex is intensified in the descending rear-to-front (RTF) inflow as a result of continued sublimative melting and evaporative cooling in the stratiform region. It decouples from the front-to-rear (FTR) ascending and anticyclonic flow in the upper troposphere during the formative stage. The vortex tilts northward with height, resulting in a deep layer of cyclonic vorticity (up to 250 mb) near the northern end of the squall line. It has an across-line scale of 120–150 km and a longitudinal scale of more than 300 km, with its maximum intensity located above the melting level.

A three-dimensional vorticity budget shows that the cooling-induced vortex is initially maintained through the vertical stretching of its absolute vorticity associated with the short-wave trough. As the descending rear inflow develops within the system, the tilting of horizontal vorticity is about one order of magnitude larger than the stretching in determining the early intensification of the vortex. In most vortex layers, the stretching tends to destroy the vortex locally, owing to the existence of the divergent outflow in the lower troposphere. Only when the vortex propagates into the FTR–RTF flow interface does the stretching effect begin to control the final amplification of the vortex, and the tilting plays a negative role during the squall's decaying stage.

The model also reproduces well a narrow heating-induced (or warm-core) cyclonic vortex along the leading convective line and a deep anticyclonic-vorticity zone between the heating- and cooling-induced mesovortices. It is shown that the cyclonic vortex along the leading line develops through positive tilting and stretching, whereas the anticyclonic-vorticity zone is generated by tilting of horizontal vorticity by the FTR-ascending and RTF-descending flows, and later enhanced by negative stretching along the interface convergence zone. The warm-core vortex dissipates and eventually merges into the cooling-induced vortex circulation as the system advances into a convectively less favorable environment. The anticyclonic-vorticity zone rapidly diminishes as the cooling-induced vortex moves into the flow interface. At the end of the life cycle, the cooling-induced mesovortex becomes the only remaining element of the squall system that can be observed in a deep layer and at a larger scale in the low to midtroposphere. Different characteristics of heating-induced versus cooling-induced mesovortices and their relationships are discussed. The results suggest that mesovortices are ubiquitous in MCS's and that their pertinent mesoscale rotational flow may be the basic dynamic effect of MCS's on their larger-scale environments.

1. Introduction

Because of various special datasets, the intense squall line that occurred on 10–11 June 1985 during Preliminary Regional Experiment for STORM-Central (PRE-STORM) (see Cunning 1986) has been the subject of numerous investigations [e.g., Augustine and Zipser 1987; Rutledge et al. 1988; Johnson and Hamilton 1988 (JH); Zhang et al. 1989 (ZGP); Zhang and Gao 1989 (ZG); Houze et al. 1989; Biggerstaff and Houze 1991a,b (BH)]. These observational and numerical studies have led to a much better understanding of the internal structure and evolution of the squall line and of mesoscale convective systems (MCS's) in general. These structural features include the development of descending rear inflows and their relationship to surface wake lows, the formation of trailing stratiform precipitation, and the generation of surface pressure perturbations and internal circulation characteristics.

Corresponding author address: Dr. Da-Lin Zhang, Department of Meteorology, McGill University, 805 Sherbrooke Street West, Montreal, Quebec H3A 2K6, Canada.

Much, however, remains to be understood about the midlevel mesovortex[1] that formed in the trailing stratiform region of the squall system. Although ZGP showed the development of such a salient mesoscale feature from both the simulation and (rawinsonde) observations, their study primarily focused on the verification of the simulation against observations. With composite observations, BH documented some kinematic structures of the mesovortex, but their results apply only to a 5-h period during the mature stage of the storm's development. It is of particular interest that the present mesovortex was induced by latent cooling in a descending rear-inflow jet (see Fig. 8 in Zhang and Cho 1992), as opposed to warm-core mesovortices that form in ascending flow of MCS's (e.g., Bosart and Sanders 1981; Zhang and Fritsch 1987, 1988b; Kuo et al. 1988; Menard and Fritsch 1989). Whether mesovortices developed in the descending or ascending portion of MCS's is rather ambiguous from previous observational studies.

The origins and subsequent intensification mechanisms of mesovortices in the stratiform region of MCS's also appear in a matter of controversy in the recent literature. For instance, the first direct satellite investigations of 26 mesovortices by Johnston (1981) simply stated that they "originated someplace within mesoscale convective complexes" (Maddox 1980). Smull and Houze (1985) and Stirling and Wakimoto (1989) attributed mesovortices that resulted in "notch" echoes in the trailing stratiform region during the system's decaying stage to the splitting of an existing larger-scale mesovortex. Zhang and Fritsch (1987) argued that the presence of strong environmental angular momentum associated with a low-level jet could assist the concentration of cyclonic vorticity. Zhang and Fritsch (1987, 1988b), Kuo et al. (1988), and Menard and Fritsch (1989) showed that the low- to midlevel convergence associated with latent heat release was primarily responsible for the rapid development of mesovortices within mesoscale convective complexes (MCCs). Numerical simulations by Wu and Chen (1985), Wang and Orlanski (1987), and Kuo et al. (1988) indicate that mesovortices could develop in association with the terrain-induced standing eddies or lee troughs. More recently, Bartels and Maddox (1991) studied composite characteristics of more than 20 mesovortices identified by visible satellite imagery and suggested that the vertical stretching of planetary vorticity might be the dominant mechanism for the initial spinup of midlevel circulations. With the PRE-STORM datasets, Brandes (1990) and Johnson and Bartels (1992) found that the midlevel convergence associated with a mesoscale updraft–downdraft couplet in the stratiform region played a key role in the generation of mesovortices in the midtroposphere. Brandes (1990) also mentioned that cyclonic vorticity could be generated by tilting horizontal vorticity associated with low-level horizontal temperature gradients across the mesovortex. Verlinde and Cotton (1990) noted from dual-Doppler radar data that mesovortices could be produced by the upward transport of low-level momentum by multiple convective updrafts (i.e., the tilting effect) rather than by vertical motion within the stratiform region. Biggerstaff and Houze (1991b) concluded from their composite analysis that tilting of horizontal vorticity by gradients of dry rear-inflow subsidence at the back edge of the stratiform region was a factor of 2–10 greater than stretching of vertical vorticity in the development of the 10–11 June 1985 mesovortex.

Nevertheless, previous studies have revealed a variety of interesting kinematic and thermodynamic characteristics of midlevel mesovortices. The typical vortex circulations range from 50 to 300 km in diameter (Johnston 1981; Stirling and Wakimoto 1989; Bartels and Maddox 1991) and last from a couple of hours to several days (Verlinde and Cotton 1990; Bosart and Sanders 1981; Wetzel et al. 1983; Murphy and Fritsch 1989). The level at which cyclonic vorticity concentrates also differs; for example, from near the melting level (Ogura and Liou 1980; Gamache and Houze 1982; Zhang and Fritsch 1988b; Menard and Fritsch 1989; BH; Johnson and Bartels 1992) to a deep layer in the low to midtropospheres (Bosart and Sanders 1981; Zhang and Fritsch 1987; Leary and Rappaport 1987; Brandes 1990). The vertical distribution of vortex properties varies from nearly upright to downstream tilt (Zhang and Fritsch 1988b; Johnson and Bartels 1992). Another ambiguity associated with mesovortices is the relationship between their vertical thermal structures and kinematic characteristics. Specifically, some mesovortices have been reported to coexist with a warm core in the midtroposphere (Zhang and Fritsch 1987, 1988b; Kuo et al. 1988; Bartels and Maddox 1991), whereas others have been observed to have a warm anomaly at a level about 100 to 200 mb above the surface (JH; ZGP; Johnson and Bartels 1992). As will be seen in this study, knowledge of three-dimensional (3D) thermal structure is instrumental in determining the processes that lead to the midlevel mesocyclogenesis.

Although the number of studies of mesovortices has grown considerably in recent years, especially after PRE-STORM, there has been little discussion about the development of cooling-induced mesovortices in

[1] Mesovortices are defined, following Zhang and Fritsch (1987), as significant concentrations of positive relative vorticity of magnitude at least that of the local Coriolis parameter, eventually leading to the formation of a closed circulation. Mesovortices that exhibit spiral cloud signature in satellite imagery have alternatively been referred to as mesoscale vorticity centers (MVCs, Johnston 1981), rotating MCS's (Zhang and Fritsch 1988b), and mesoscale cyclonic vortices (MCVs, Bartels and Maddox 1991). These definitions appear to imply different scales, as discussed in the text.

the descending portion of MCS's. Thus, it still remains vague as to how this type of midlevel mesovortex can materialize due to diabatic cooling in descending flow. How do they differ from warm-core mesovortices? Why are there different types and scales of vortex circulations occurring within MCS's? What are their 3D kinematic and thermodynamic structures and evolution? What are their relationships to the development of stratiform precipitation and to the life cycle of the MCS's in which they are embedded? How do they interact with mesoscale circulations in the lower and upper troposphere? Recent observational studies have provided encouraging evidence, but insufficient information, on the development of mesovortices within MCS's. In fact, currently accessible observations, including those from PRE-STORM, allow only limited efforts to investigate the above issues, owing to either inadequate resolution or incomplete measurements in both temporal and spatial coverages, or a lack of dynamic consistency between the mass and wind fields.

The objective of the present study is an attempt to address the aforementioned questions through a comprehensive examination of a midlevel cooling-induced mesovortex that developed in the stratiform region of the 10–11 June 1985 squall system, primarily based on a 20-h simulation (i.e., from 1200 UTC 10 June to 0800 UTC 11 June) of the case (see ZGP and ZG). These simulation data are particularly useful for the present study because they provide a high-resolution, dynamically consistent dataset for investigating the life cycle of the mesovortex as well as its relationships to the squall system. The presentation of the results is organized as follows. Section 2 describes briefly the case and the associated model simulation. Section 3 presents the kinematic structure and evolution of the mesovortex using both the model simulation and available observations. Section 4 shows the cause and effect of the mesovortex, based on the thermodynamic structure obtained from the high-resolution simulation. Section 5 examines possible mechanisms whereby the present mesovortex developed in the wake of the system through a detailed budget computation of absolute vorticity. Section 6 synthesizes the present study with previous vortex investigations and discusses how different types of midlevel mesovortices could be convectively generated. A summary and concluding remarks are given in the final section.

2. Case description

The squall line of our interest was initiated at 2100 UTC (1500 LST) 10 June 1985 as a weak surface front moved toward the PRE-STORM network and interacted with a thermal boundary (See JH and ZGP). Then the system intensified rapidly within a widespread convectively unstable environment over the network and advanced southeastward at a speed of 14–16 m s^{-1}. The mesovortex under investigation was observed to develop to the north of the convective line (see ZGP and BH). Both the satellite imagery and radar echoes display rapid expansion of stratiform cloudiness over the area where the mesovortex was located (Rutledge et al. 1988). The squall system entered the mature and nearly steady state around 0300 UTC 11 June.

For the numerical simulation, an improved nested-grid version of the Pennsylvania State University–National Center for Atmospheric Research (NCAR) Mesoscale Model (Anthes et al. 1987) with a fine-mesh grid size of 25 km was utilized, in which a modified version of the Fritsch–Chappell (1980) cumulus parameterization scheme and explicit calculations of cloud water (ice) and rainwater (snow) were simultaneously incorporated (Zhang 1989). ZGP and ZG showed that the model reproduced many internal structures and the evolution of the 10–11 June 1985 squall system extremely well with *conventional data,* as verified against observational analyses by Augustine and Zipser (1987), JH, and Rutledge et al. (1988). Specifically, the model simulates well the initiation of the squall line at nearly the right time and location; the orientation and propagation of the squall system; the relative flow configuration of front-to-rear (FTR) motion at both upper and lower levels with an intermediate rear-to-front (RTF) inflow; and the location, flow structure, and strength of the mesovortex. In addition, BH's composite analysis of the squall's vorticity structure enhances further the credibility of this model simulation. Therefore, this high-resolution simulation provides a great opportunity for a more detailed investigation of the mesovortex than is possible even with the PRE-STORM dataset. For a comprehensive description of the case and the model simulation, the reader is referred to the above cited publications.

3. Kinematic analysis

As ZGP showed, two regions of cyclonic-vorticity concentrations appear in the 10–11 June 1985 squall system: one originates from the surface cold front at the model initial time (i.e., 1200 UTC 10 June), and the later penetrates into a deep layer in the troposphere, owing to the continued convective development along the leading line (Figs. 28 and 31b in ZGP); another is initially associated with a midlevel traveling short wave (see Fig. 3 in ZGP), and later occurs in the middle troposphere in the trailing stratiform region of the system (Figs. 29a, 30, and 31b in ZGP). These two cyclonic-vorticity concentrations will be hereafter referred to as "the leading vortex" and "the wake vortex," respectively, according to their relative positions in the squall system. Biggerstaff and Houze (1991b) also found the development of such a vortex couplet from their composite analysis. In addition, BH analyzed an

elongated anticyclonic-vorticity zone between the couplet. As will be shown, these internal structures appear in the present model simulation, too; the wake vortex, however, will be the focus of the present study.

Figures 1a–c show the time evolution of midlevel absolute vorticity, superposed with divergence (dotted lines) and relative wind vectors valid at 0000, 0300, and 0600 UTC 11 June 1985, respectively. The three periods are selected to represent the initiation, mature, and dissipation stages of the squall system. In order to make the vortex structure evident, the system's movement of 14.5 m s^{-1} toward 135° has been subtracted from the flow. From Figs. 1a,b, the aforementioned structure of a leading vortex followed by a wake vortex is quite evident during the initiation and mature stages. Moreover, there is an elongated zone of negative relative vorticity between the vortex couplet. This anticyclonic vorticity, as will be shown in Fig. 4, is more pronounced at higher levels. During the initiating stage, the relative flow shows little sign of a closed circulation associated with the wake vortex. Three hours later, the wake vortex, with its center denoted by the letter "V" (similarly in the rest of the figures), rapidly intensifies from 2.1 to 3.7 $\times 10^{-4}$ s^{-1} (in absolute vorticity), and also expands in scale from roughly 50 to 150 km in diameter (based on the 2×10^{-4} s^{-1} contour). Because of the development of strong RTF and FTR currents during the mature stage (see ZG), a "closed" relative wind circulation[2] occurs at a scale much larger than that defined by vorticity (here referred to footnote 1). The development of the closed wind circulation conforms to rawinsonde observations for this case. As Fig. 2 shows, the observed actual winds also indicate a closed circulation at 600 mb behind the leading line. It is clear that even with the supplemental rawinsondes during PRE-STORM, any objective analysis of the observations would fail to resolve the vortex couplet as well as the intermediate anticyclonic-vorticity zone (cf. Figs. 1b and 2).

As the system enters the dissipating stage (Fig. 1c), the leading vortex weakens markedly, as does the leading convective line (see ZGP); it only contains significant cyclonic vorticity below 600 mb, as will be shown in Fig. 4. In contrast, the wake vortex continues to intensify, despite the fact that its relative vorticity had already increased by a factor of 5 since the initiation of the squall line. While the wake vortex intensifies considerably during the mature-to-decaying stage, its across-line dimension remains similar to that 3 h before. The vortex-related wind circulation, however, occurs over an area much larger than that occupied by the squall system. The larger-scale wind circulation apparently results from the development of extensive RTF inflow in conjunction with the cyclonic flow occurring to the northern edge of the system. It is evident that the intensification of the RTF inflow assists the concentration of cyclonic vorticity along the interface (see ZG for more detailed discussion). On the other hand, the amplification of the wake vortex would in turn help enhance the RTF inflow, since the latter is part of the vortex circulation. This complementary process can be evidenced by the fact that the RTF-descending flow is relatively stronger to the south of the vortex (Fig. 1c), whereas to its north, the RTF flow is both weak and elevated (see Fig. 5 in ZG). Of course, without vorticity sources or sinks, mesovortices would behave just like passive entities that are driven by atmospheric flow.

Note the relative position of the wake vortex with respect to the convergence zone associated with the FTR-ascending and RTF-descending couplet. Initially, a large portion of the low- to midlevel convergence zone coincides with *the leading vortex,* which provides the forcing necessary for the rapid development of deep convection along the leading line. Later, this convergence zone gradually becomes in phase with *the wake vortex,* particularly during the decaying stage. This implies that vortex stretching may play different roles in the amplification of the wake vortex during the life cycle of the squall system. This point will be examined in detail in section 5.

Figure 3 illustrates the time evolution of the wake vortex (dashed lines) in relation to the leading vortex (solid lines) since the initiation of the squall line. The leading vortex axis is centered along the low-level RTF actual flow immediately behind the gust front (see Figs. 12 and 15–16 in ZGP). Examination of the hourly model output reveals that the wake vortex, located over northeastern Colorado at 2200 UTC, originates from the cyclonic vorticity associated with the midlevel short-wave trough. Of particular importance here is that the distance between the centers (or axes) of the wake and the leading vortices shortens as the squall system propagates southeastward (Fig. 3). Furthermore, the shortening accelerates during the system's decaying stage, as can also be seen from Figs. 1a–c. This implies that the wake vortex tends to overtake the leading vortex as well as the convective line. As will be presented in section 5, the overtaking process has prominent implications for the rapid intensification of the wake vortex during the squall's decaying stage.

Figures 4a–d display vertical cross sections of absolute vorticity, divergence (dotted lines), and relative flow vectors valid at 2200 UTC 10 June, 0000, 0300, and 0600 UTC 11 June, respectively. These cross sections are taken through the vortex center and are nearly perpendicular to the leading line (see dotted lines in Fig. 3), except for the 2200 UTC diagram, which was purposely taken across the wake vortex and the leading

[2] As will be shown in Fig. 4, the FTR and RTF flows that form this closed horizontal circulation are bifurcated along the flow interface in vertical cross sections.

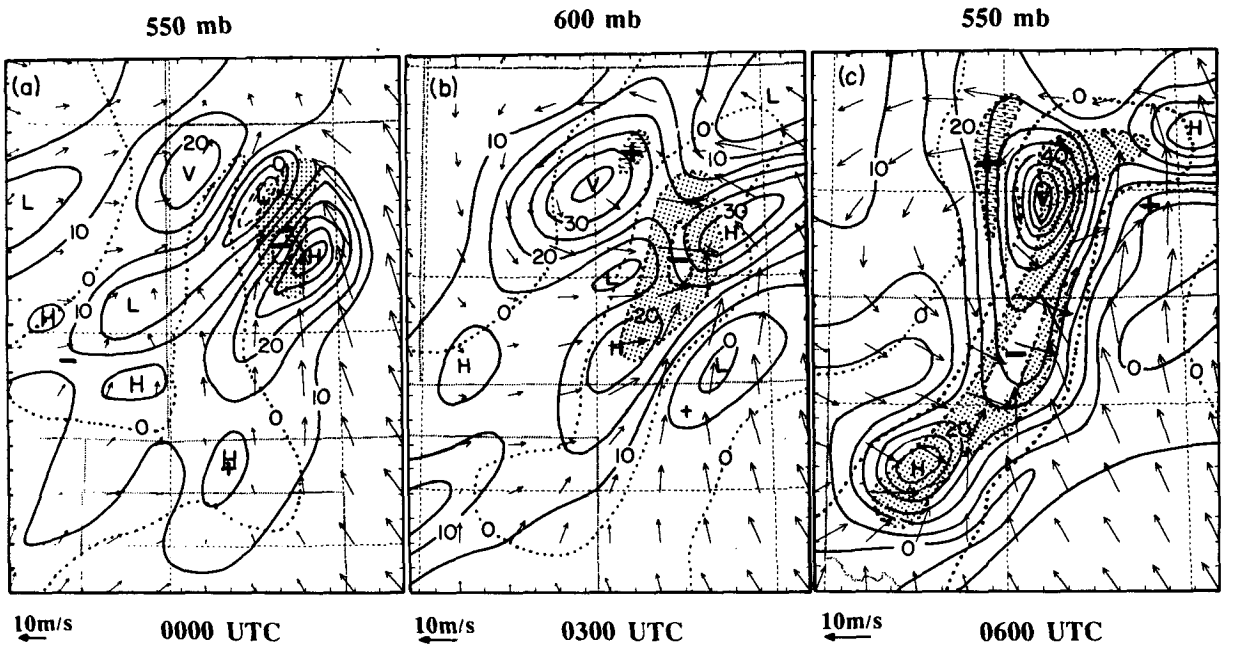

FIG. 1. The distribution of absolute vorticity (solid lines—positive, dashed lines—negative) at intervals of 5×10^{-5} s^{-1}, divergence (dotted lines) at intervals of 2×10^{-4} s^{-1}, superposed with relative wind vectors at (a) 550 mb from 12-h simulations; (b) 600 mb from 15-h simulations; and (c) 550 mb from 18-h simulations over model subdomains, valid at 0000, 0300, and 0600 UTC 11 June 1985, respectively. The letter V denotes the core of the wake vortex; the signs "+" and "−," denote the local maximum of divergence and convergence, respectively; similarly, in the rest of the figures. The intervals marked on the frame are mesh grids of 25 km. Shadings and hatchings denote areas of divergence and convergence larger than 2×10^{-4} s^{-1}, respectively.

updraft–vortex centers. It is apparent that the simulated internal circulations resemble well the 2D conceptual model of a squall line byu Houze et al. (1989), particularly during the mature-to-decaying stage.

At 2200 UTC (i.e., 1 h after the initiation of the squall line), the leading cyclonic-vorticity concentrates

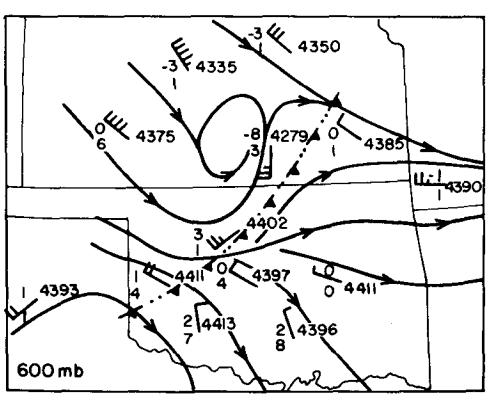

FIG. 2. Streamline analysis of the 600-mb actual winds based on the 0300 UTC 11 June 1985 observations over the PRE-STORM network. A full barb is 5 m s^{-1}. Cold-front symbols alternated with double dots indicate the distribution of surface outflow boundaries.

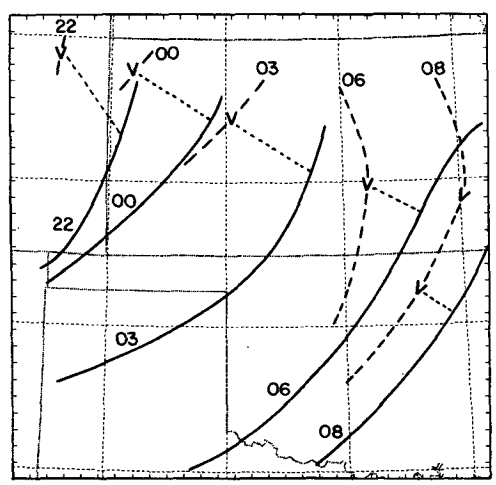

FIG. 3. The time evolution of the leading vortex (solid lines) at a level about 100 mb above the surface (i.e., $\sigma = 0.873$) and the wake vortex (dashed lines) in the middle troposphere from 2200 UTC 10 June 1985 to 0800 UTC 11 June 1985. Here σ is the vertical coordinate and defined as $\sigma = (p - p_t)(p_s - p_t)^{-1}$, where p_t is the pressure at the top of the model atmosphere (80 mb in this case) and p_s is the surface pressure. The vortex axes are based on the absolute vorticity contour of 2×10^{-4} s^{-1}. The dotted lines denote the portions of vertical cross sections used, and the letter V indicates the relative location of the wake vortex, in subsequent figures to reveal the vortex structures.

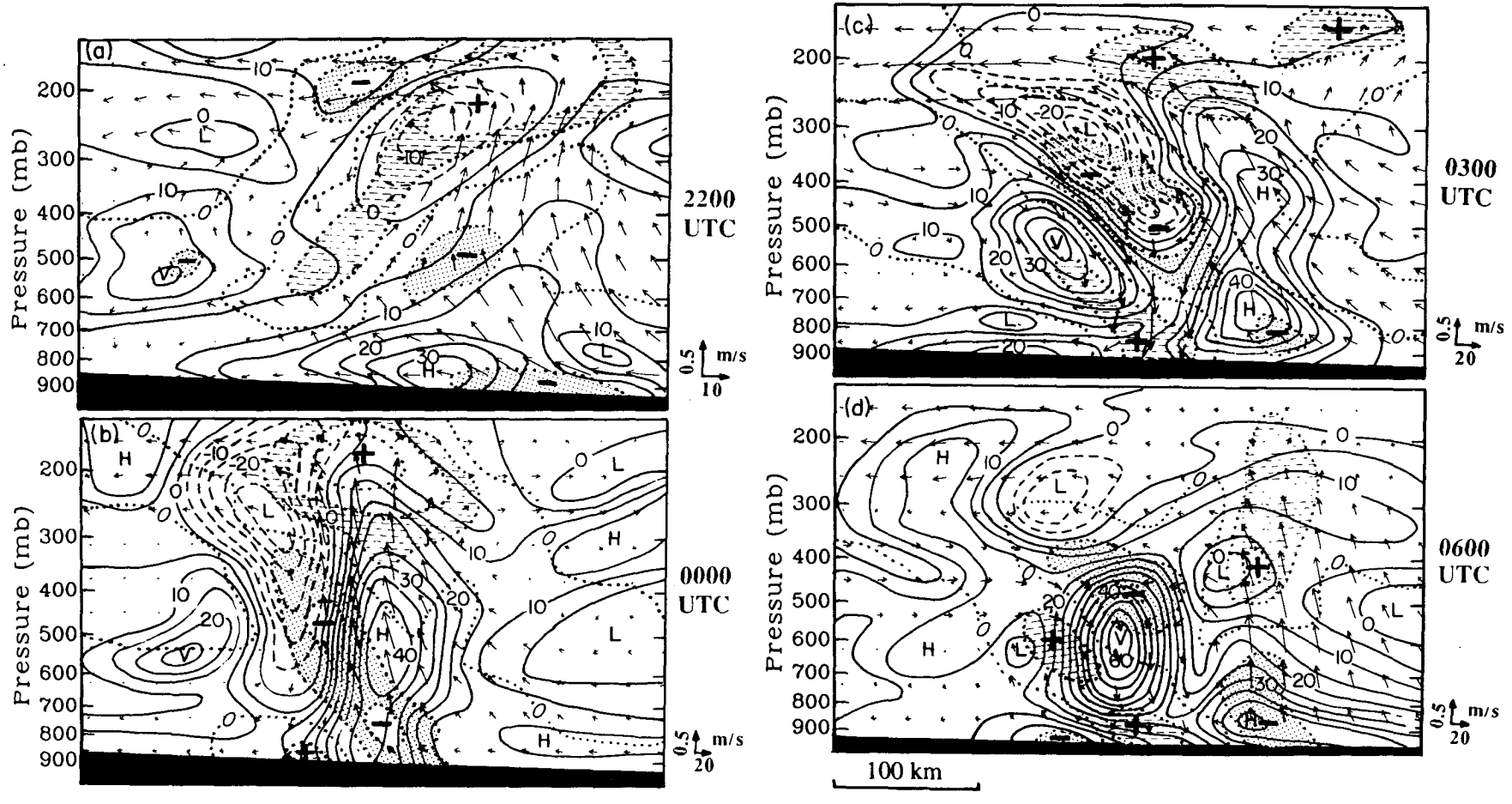

FIG. 4. Vertical cross sections of absolute vorticity (solid lines—positive, dashed lines—negative) at intervals of 5×10^{-5} s^{-1}; divergence (dotted lines) at intervals of 2×10^{-4} s^{-1} except for the 10 h-simulation in which an interval of 10^{-4} s^{-1} is used, superposed with relative across-line flow vectors along lines through the core of the wake vortex, as given in Fig. 3 from (a) 10-h simulations, (b) 12-h simulations, (c) 15-h simulations, and (d) 18-h simulations, valid at 2200 UTC 10 June 1985 and 0000, 0300, and 0600 UTC 11 June 1985, respectively. Shadings and hatchings represent areas of convergence and divergence larger than 2×10^{-4} s^{-1}, respectively, with their centers denoted by the respective signs of "−" and "+," except for the 10-h simulation in which the value of 10^{-4} s^{-1} is used.

along a shallow surface cold front, in coincidence with a favorable convergence zone with continued convective development (Fig. 4a). In contrast, the wake vortex is embedded in a weak convergence zone associated with the midlevel meso-α-scale short wave (cf. Fig. 3 in ZGP and Fig. 4a herein), so that it is more or less maintained by the stretching of its absolute vorticity. Both vortices are evidently weak to begin with at this time. Once the squall system intensifies, however, this vortex couplet assumes totally different characteristics of evolution. It is of particular interest that the development of the leading vortex is strongly linked to the ascending motion along the leading convective line, whereas *the wake vortex intensifies in a descending rear inflow* (Figs. 4b–d). Specifically, the leading vortex strengthens rapidly as the leading upward motion increases; it also dissipates rapidly as the system advances into a convectively less unstable environment and the leading updrafts weaken (see ZGP). On the contrary, the most rapid development of the wake vortex occurs during the system's decaying stage, when it has come into phase with the convergence zone along the interface. At 0600 UTC, the wake vortex is nearing its maximum intensity and spatial coverage, while the leading line and its attendant vortex are dissipating rapidly. This feature explains why the wake vortex tends to be better observed during the decaying stage of MCS's (e.g., Smull and Houze 1985; Stirling and Wakimoto 1989; Johnson and Bartels 1992).

Several other interesting phenomena in Fig. 4 are also worthwhile to mention. First, the wake vortex attains its maximum intensity at 550 mb, rather than below the melting level (i.e., at 600 mb in the present case), as in the BH conceptual model. As will be shown in sections 4 and 5, the wake vortex develops through tilting by descending rear inflow and stretching by midlevel convergence; both are mainly determined by the mid- to upper-level cooling associated with sublimation, evaporation, and melting. Thus, intuitively speaking, the wake vortex should have its strongest intensity occurring *above* the level of maximum cooling, as opposed to latent heating-driven mesovortices that tend to have the greatest cyclonic vorticity *below* the level of maximum heating. This implies that with additional cooling due to melting, wake vortices would more likely have their maximum intensity above the melting level if contributions from other processes are small. Second, as previously mentioned, the wake vortex advances gradually into the leading edge of descending rear inflow from far behind (Figs. 4a–c), and during the decaying stage, it comes into phase with the convergence zone along the interface (Fig. 4d). The maximum convergence occurs above the core of the wake vortex. Third, a region of anticyclonic vorticity occurs in a deep layer of the middle to upper troposphere centered along the interface during the intensifying stage. This, to a certain extent, supports BH's conceptual model. A vertical cross section taken to the south of the vortex center, which represents better the squall's linear structure, shows that the strongest negative vorticity is located in the upper troposphere (see Fig. 8 in Zhang and Cho 1992). This negative vorticity can be understood as a result of up- and rearward transport of the low-level convectively unstable air along the sloping FTR flow, based upon the conservation of moist potential vorticity (MPV) (Zhang and Cho 1992). Note that the middle portion—but not the upper portion—of the anticyclonic vorticity rapidly diminishes as the system enters the decaying stage (Fig. 4d). Lastly, beneath the wake vortex is a shallow layer of relative anticyclonic vorticity close to the surface that persists even during the decaying stage. This feature is more pronounced in the southern portion of the squall's stratiform region (see Fig. 5). As will be shown in section 5, this relative anticyclonic vorticity is produced principally by the negative stretching associated

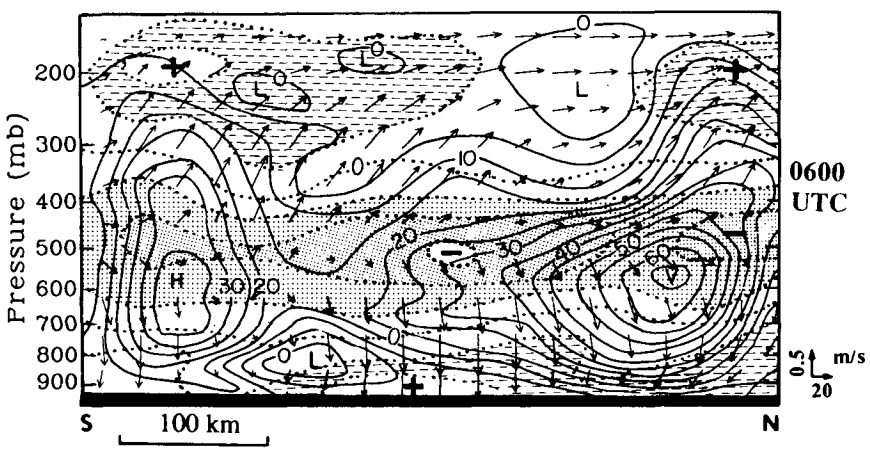

FIG. 5. As in Fig. 4d but for the curved vertical cross section along the axis of the wake vortex (referred to Fig. 1c), superposed with along-line flow vectors.

with divergent outflow and thus is distinct from that at the mid-to-upper levels.

After showing the two-dimensional (2D) across-line structure and evolution of vortices, it is necessary to discuss briefly the along-line variability and 3D aspects of the wake vortex. Thus, Fig. 5 displays the *curved* vertical cross section of absolute vorticity, superposed by along-line flow vectors, along the axis of the wake vortex at 0600 UTC. The model simulates well the generally weak ascending motion above 500 mb and the strong descending flow below in the stratiform region. Another vortex center develops on the southern end of the line, as also can be seen from Fig. 1c. This vortex corresponds to both the simulated and the observed surface mesohighs as well as to wake lows in the southern part of the squall system during this period (see Fig. 13e in JH and Fig. 16 in ZGP).

Note that the wake vortex slopes northward with height (Fig. 5) and has produced a deep layer of cyclonic vorticity in the troposphere. Such a deep layer of cyclonic vorticity tends to develop near the northern end of the squall line (see Fig. 1) as a result of the tilting of along-line vorticity, as will be seen in section 5. A similar scenario appears to have also occurred in the 23–24 June MCS during PRE-STORM (Johnson and Bartels 1992). The longitudinal dimension of the wake vortex is more than 300 km. Note also a deep layer of convergence in the midtroposphere that begins near 350 mb and peaks near 500 mb. Below 700 mb is the uniformly distributed, divergent descending outflow. Thus, the results shown in Fig. 4 represent well the 2D properties of the wake vortex; the wake vortex, however, is 3D in character. In particular, the vortex circulation should be visualized in a 3D framework, because the FTR and RTF flows that form a closed circulation in a horizontal plane are vertically bifurcated at the flow interface (cf. Figs. 1 and 4a). Furthermore, ZG have shown that the flow configuration differs from the Houze et al. (1989) conceptual model when the vertical cross section is taken at a different location (see their Fig. 5).

Since the simulated wake vortex quickly approaches the eastern boundary of the fine-mesh domain after 0600 UTC, a vertical cross section through a secondary, local vorticity center of the wake vortex at 0800 UTC is given in Fig. 6 in order to show the relation of the wake vortex to the squall's internal circulations near the end of the life cycle. It is evident that both the wake and the leading vortices have nearly merged into one entity that tilts rearward along the interface. Zhang and Fritsch (1988b) also showed an example of the downstream tilt of a simulated mesovortex pertaining to an MCC. The rearward tilt of the wake vortex in the present case is again due to the presence of strong vertical shear associated with FTR and RTF flows that tends to distort the vortex slantwise into a deeper (up to 250 mb) and wider region. Note that the wake vortex continues to accelerate forward due to the presence of the RTF relative flow, now with its core located ahead of the convergence center. Furthermore, its maximum vorticity center has been displaced downward from 550 to 650 mb (i.e., below the melting level) at this time. As will be shown in section 5, the downward displacement is due to the downward vorticity advection by descending rear inflow. Note also that the aforementioned anticyclonic vorticity is no longer present along the interface but still appears at the top of the leading dissipated updrafts. It is of particular significance that the wake vortex becomes the only remaining element of the squall system that can be observed at a larger scale in the troposphere at the end of the squall's life cycle.

To facilitate comparison of the kinematic structure of the present vortex with other relevant studies, Fig.

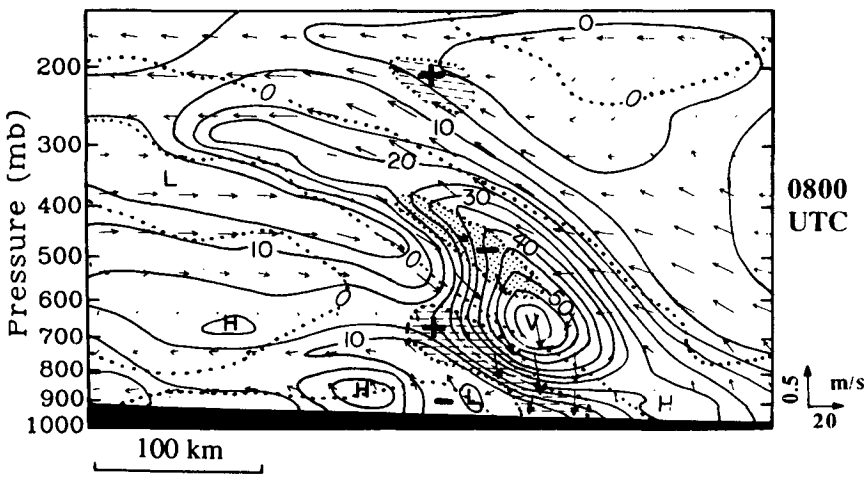

FIG. 6. As in Fig. 4d but through a secondary local vorticity center of the wake vortex, as indicated in Fig. 3 from 20-h simulation, valid at 0800 UTC 11 June 1985.

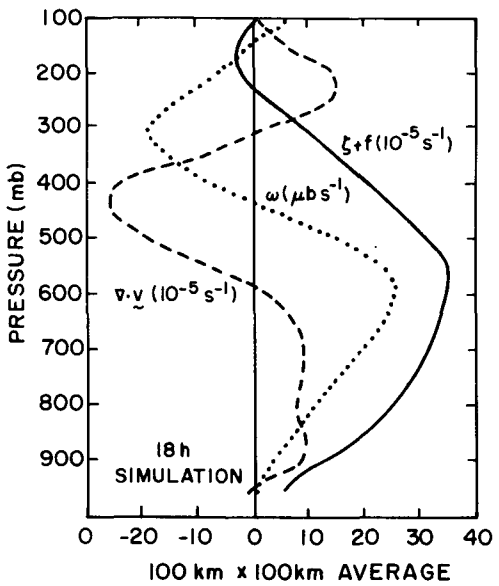

FIG. 7. Vertical profiles of absolute vorticity (10^{-5} s^{-1}, solid line), divergence (10^{-5} s^{-1}, dashed line), and ω (μb s^{-1}, dotted line) averaged over a 100-km × 100-km area centered on the wake vortex from 18-h simulation, valid at 0600 UTC 11 June 1985.

7 shows the 0600 UTC vertical profiles of absolute vorticity (solid line), divergence (dashed line), and vertical motion (dotted line) averaged over an area of 100 km × 100 km centered on the wake vortex. All profile shapes bear excellent resemblance to that obtained from observational analyses (e.g., Brandes 1990; Johnson and Bartels 1992). Maxima in vorticity and $-\omega$ occur at 550 and 600 mb, respectively. The ω profile shows the typical vertical distribution of mesoscale updrafts overlying mesoscale downdrafts in a stratiform region of MCS's. The averaged descending motion initiates around 450 mb, where extensive, trailing rear inflow meets with the FTR flow and strong convergence occurs. Then the magnitude of convergence decreases sharply downward as the descending motion increases until the flow becomes more uniformly divergent in the lower portion of the vortex. The ω and relative vorticity[3] profiles suggest that the upward extension of the wake vortex is limited by the trailing descending flow because the ascending flow above the vortex contains anticyclonic relative vorticity (also see Figs. 4b–d). Since the area being averaged covers most of the wake vortex in its across-line dimension, these profiles should reflect well the pertinent vortex characteristics, except for the portion above 450 mb, which has little kinematic relation to the development of the wake vortex, as will be further shown in the next section.

[3] For the present case, relative vorticity can be obtained roughly by subtracting the planetary vorticity $f = 9 \times 10^{-5}$ s^{-1} from absolute vorticity.

4. Thermodynamic structure

Since the wake vortex intensifies in the midtropospheric descending flow, a detailed thermodynamic analysis is essential to determine the mechanisms whereby it forms. Thus, Figs. 8a–c show the respective 0600 UTC distribution of the vertical motion [i.e., ω (μb s^{-1})] near the top of the wake vortex (i.e., at 400 mb), the geopotential height (solid lines) and temperature (dashed lines) at the level of the vortex core (i.e., 550 mb), and the vertical motion (dashed lines) and temperature (solid lines) at a lower level (i.e., σ = 0.873, about 100 mb above the surface). The model simulates a 70-km-wide updraft band along the leading line (Fig. 8c), and a 180-km-wide ascending region at the upper levels associated with both "convective" and stratiform latent heating (Fig. 8a). The simulated narrow (~50 km) and wide (~90 km) regions of descending motion at the respective upper and lower levels also appear to be realistic (cf. Figs. 8a and 8c), as compared to observational analyses of JH and BH. In the midtroposphere, a southwest–northeast-oriented meso-α-scale short-wave trough, as previously mentioned, is situated along the stratiform region, with its axis slightly lagging behind the axis of the wake vortex (cf. Figs. 8b and 1c). This short-wave trough has intensified as a result of the development of the squall system (cf. Figs. 3 and 29b in ZGP). Several studies have also reported a short-wave trough in association with the formation of a mesovortex (e.g., Zhang and Fritsch 1987, 1988b; Bartels and Maddox 1991; Johnson and Bartels 1992; Chen 1990). This is clearly due to the favorable cyclonic vorticity possessed by the trough for the generation of mesovortices. Ahead of the short-wave axis is a band of warm anomaly associated with "convective" updrafts and latent heat release along the leading line, followed by a band of cold anomaly associated with mesoscale downdrafts and sublimative–evaporative cooling along the elongated wake vortex (cf. Figs. 8b and 1c). Evidently, cold advection behind the short-wave trough could also contribute to the cooling in the stratiform region. In contrast, the lower portion of the wake vortex is characterized by a large area of significant warming (about 5°C, see Fig. 8c), with a narrow zone of the evaporatively generated cold pools located ahead of it. Beneath this warm anomaly is a hydrostatically generated wake low pressure (see JH and ZGP). This upper-level cooling and low-level warming has often been observed as a shallow layer of nearly vanishing to negative lapse rates in the midtroposphere in association with the so-called "onion-shaped" soundings (e.g., Fig. 8 in Zipser 1977; Fig. 17 in JH; Fig. 23 in ZGP; Fig. 11 in Johnson et al. 1989; Fig. 6 in Brandes 1990). This vertical thermal structure suggests that the thermal wind relationship is completely inapplicable to this situation, since it would indicate an anticyclonic circulation with a midlevel cold anomaly.

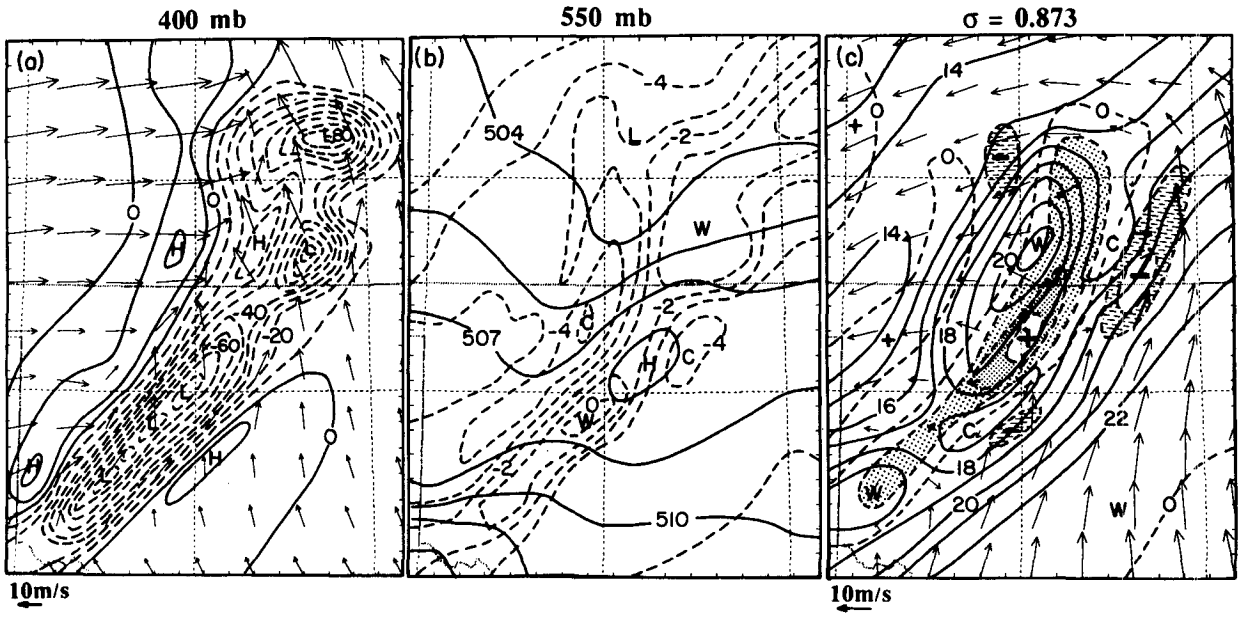

FIG. 8. Distribution of (a) ω (solid line—positive, dashed lines—negative) at intervals of 10 μb s^{-1} superposed with relative flow vectors at 400 mb; (b) geopotential height (dam, solid lines) at intervals of 15 dam and temperature (dashed lines) at intervals of 1°C at 550 mb; and (c) temperature (solid lines) at intervals of 1°C and ω (dashed lines) at intervals of 10 μb s^{-1} superposed by relative-flow vectors at a level about 100 mb above the surface (i.e., σ = 0.873, see Fig. 3 caption for the definition), from 18-h simulation, which is valid at 0600 UTC 11 June 1985. The letters W and C denote the centers of warm and cold anomalies, respectively. Shadings and hatchings in Fig. 8c denote downward and upward motion, respectively, with their centers denoted by the respective signs of "+" and "−."

It is apparent that the mid- to upper-level cooling tends to destabilize the atmospheric column gravitationally, and descending motion will be expected to develop rapidly. Zhang and Gao (1989) illustrated that 1) the large-scale baroclinity tends to produce the trailing RTF flow within the upper portion of the troposphere; 2) midlevel mesolows induced by the warming in updraft regions assist the forward (rearward) acceleration of the RTF (FTR) flow; and 3) the sublimative melting and evaporative cooling is responsible for the descending portion of the RTF flow. In the present case, Figs. 7 and 8a show that this sinking motion is initiated near 400 mb behind the interface as the westerly flow enters the trailing stratiform region, while Fig. 9 shows that a pocket of dry air is associated with the RTF descending inflow. Hence, the extensive trailing RTF inflow provides a source of dry air that tends to cause sublimative cooling along the leading edge of descending flow, melting near 600 mb and evaporative cooling below. This cooling would then enhance the descending component of the RTF flow and midlevel convergence (ZG, Lafore and Moncrieff 1989). Since the descending rear inflow is part of the vortex circulation, *the wake vortex can be considered as being directly induced by mid- to upper-level latent cooling,* rather than by latent heating in the FTR ascending flow. The next section provides further evidence, through a vorticity budget, pointing to the same conclusion. Note a sloped cold ridge that has been produced along the leading edge of the descending flow as a result of the sublimative-evaporative cooling; its peak cooling occurs at a level close to the vortex core (i.e., at 550 mb; cf. Figs. 9 and 8b) and above the melting

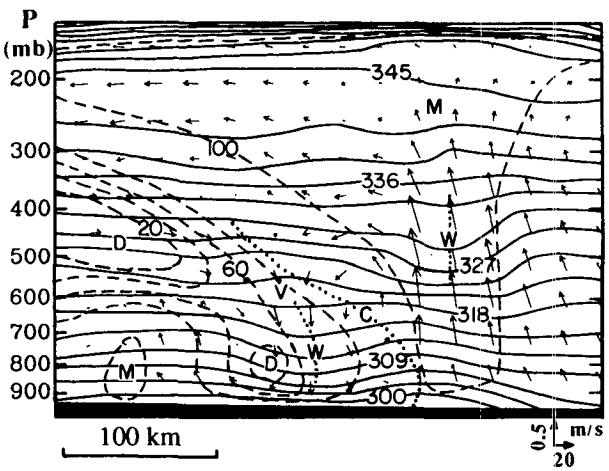

FIG. 9. Vertical cross section of virtual potential temperature (θ_v, solid lines) at intervals of 3 K, relative humidity (dashed lines) at intervals of 20%, superposed with relative across-line flow vectors from 18-h simulation, valid at 0600 UTC 11 June 1985. The letters W, C, D, M, denote the center of warm, cold, dry, and moist anomalies, respectively. The dotted lines denote vertical axes of warm or cold anomalies.

level. Because of its tendency to destabilize an atmospheric column gravitationally, this type of latent cooling and the resulting cold anomaly are unbalanced thermal structures and could merely survive for a short period, as compared to more balanced midlevel warm-core structure (e.g., Zhang and Fritsch 1987; 1988b).

Below the vortex core, the descending flow becomes more divergent (cf. Figs. 7 and 9). A cold pool closely associated with evaporative cooling builds up along the leading edge of the downdrafts, whereas right beneath the core of the wake vortex, adiabatic warming exceeds diabatic cooling because less precipitation is available for evaporation toward the rear. Relative humidity less than 40% can be seen in association with the warm anomaly in the lower portion of the wake vortex. This gives rise to an onion-shaped sounding near the center of the wake vortex, as shown in JH and ZGP. From the vertical-motion profile (Fig. 7) and thermal structure (Fig. 9), the sublimative cooling appears to play an important role in the generation of the strong descending flow and the strong wake vortex. The melting effect seems to be more significant along the leading edge of descending flow (see dotted lines in Fig. 9), where more hydrometeors are available and the air is close to saturation. These results are consistent with the 1D sensitivity study by Stensrud et al. (1991) in which the sublimative cooling accounts for the downward transport of upper-level momentum and the generation of the onion-shaped thermal structure. Because of the relationship between the descending rear inflow and the wake vortex, the mid- to upper-level cooling in the stratiform region may be regarded as the *cause* for, and the low-level warming and drying as the *effect* of, the rapid development of descending rear inflow and the wake vortex. On the other hand, the intensification of the descending rear inflow and the wake vortex would assist the generation of the mid- to upper-level cooling through transporting more dry air into the squall system. Furthermore, ZG showed that the development of trailing stratiform precipitation is instrumental in the generation of wake lows, since it provides necessary precipitable hydrometeors for producing diabatic cooling and subsequent descending motion as they fall into a dry atmospheric column. This conclusion can evidently be applied to the wake vortex. That is, *the trailing stratiform precipitation is the medium for the development of wake vortices,* and wake lows are the end product of a chain of complicated dynamic reactions from the generation of hydrometeors along the leading line to the enhanced descending rear inflow and adiabatic warming and drying.

Figure 10 presents a vertical cross section of height deviations and the equivalent potential temperature (θ_e, dotted lines) during the mature stage. Height deviations, obtained by subtracting their pressure-level averages in the cross section, display a presquall mesolow, a mesohigh associated with the cold pool, and a wake low underneath the wake vortex (see JH and ZG for more details). Although Figs. 9 and 10 are taken from different hours of the simulation, the deviation ridge and trough in the lower-half portion of the troposphere clearly correspond to the bands of the cooling and warming, respectively. There are two low pressure regions in the midtroposphere: one is related to the short-wave trough, and another is "convectively" generated and maintained by latent warming aloft. This pressure distribution resembles well that analyzed by Biggerstaff and Houze (1991a, see their Fig. 14b). The wake vortex tends to propagate roughly with the trough toward the leading edge of descending rear inflow where the maximum cooling occurs, and eventually merge with the convectively generated mesolow (see Fig. 3 ZG).

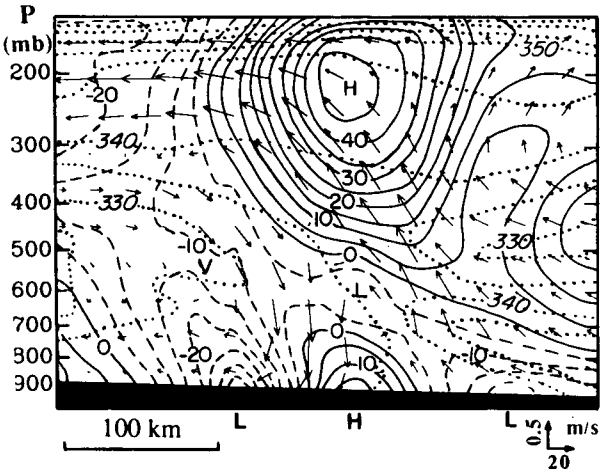

FIG. 10. Vertical cross section of height deviations (solid lines—positive, dashed lines—negative) at intervals of 5 m and the equivalent potential temperature (θ_e, dotted lines) at intervals of 5 K, superposed with relative-flow vectors from 15-h simulation, valid at 0300 UTC 11 June 1985.

It is important to note the distribution of θ_e in relation to the vertical circulations of the squall system (Fig. 10). The wake vortex is situated in a layer with relatively weak θ_e gradients that are produced as a result of continued slantwise descending motion in the stratiform region. There also exists a slantwise θ_e surface (e.g., roughly 335 K) that coincides with the interface almost all the time (also see Fig. 4 in ZG); *this surface appears to act as a material surface in separating the RTF descending flow from the FTR ascending flow.* This feature further reveals that the wake vortex has little kinematic relationship with the mesoscale circulations above the interface, except near the end of the squall's life cycle, when the entire vortex enters into the interface (see Fig. 6). Moreover, it indicates that the mid- to upper-level diabatic heating in the FTR ascending flow plays only a role in supplying energy for the development and maintenance of the whole squall system; it has little direct effect on the generation of the wake vortex during the formative stage.

5. Vorticity budget

With the dynamically consistent model dataset, a complete 3D vorticity budget for the mesovortices at different stages can be performed to provide an understanding of the processes that lead to the midlevel mesocyclogenesis. The equation describing the time rate of change in absolute vorticity following a parcel in isobaric coordinates may be written as

$$\frac{D(\zeta+f)}{Dt} = -(\zeta+f)\left(\frac{\partial u}{\partial n}+\frac{\partial v}{\partial s}\right) - \left(\frac{\partial \omega}{\partial n}\frac{\partial v}{\partial p} - \frac{\partial \omega}{\partial s}\frac{\partial u}{\partial p}\right) + \left(\frac{\partial F_s}{\partial n} - \frac{\partial F_n}{\partial s}\right) \quad (1)$$

and

$$\frac{\delta\zeta}{\delta t} = \frac{D(\zeta+f)}{Dt} - u\frac{\partial(\zeta+f)}{\partial n} - v\frac{\partial(\zeta+f)}{\partial s} - \omega\frac{\partial(\zeta+f)}{\partial p}, \quad (2)$$

where ζ is the vertical component of relative vorticity; f is the local Coriolis parameter; u, v, and ω are the *relative* wind components in the right-hand coordinates (n, s, p), respectively, with n axis normal to the line, positive in its direction of propagation; and F_n and F_s denote the numerical diffusion of horizontal momenta. The first term on the rhs of (1) is the stretching (the product of horizontal convergence and absolute vorticity), which tends to cause an exponential increase (decrease) of the existing absolute vorticity as long as convergence (divergence) is maintained. The second term on the rhs of (1) represents the tilting (twisting) of horizontally oriented vorticity into the vertical by a nonuniform vertical-motion field, which could create vorticity, provided that vertical shears are correlated with the nonuniform vertical motion. The last term on the rhs of (1) is the frictional effects due to numerical diffusion and the boundary-layer flux divergence that tend to damp the growth of positive (negative) vorticity. These three terms are the sources or sinks of absolute vorticity following an air parcel in a Lagrangian sense. It is found that the diffusion effect is small in (1), as compared to other terms (see Fig. 9 in Gao et al. 1990), and thus will be ignored in subsequent discussions. The contribution due to the planetary boundary layer has also been neglected in the budget calculations, because this effect is merely notable in the lowest 20 mb in regions where MCS's are distributed (see Fig. 9 in Gao et al. 1990). Subgrid-scale convective momentum transport was excluded in the Fritsch–Chappell cumulus scheme for the present simulation (see the related discussion in ZGP). The terms on the rhs of (2) are the vorticity sources or sinks arising from (1), relative across-line and along-line horizontal advection, and vertical advection of absolute vorticity, respectively. To separate the advective effect associated with the system translation from the dynamical processes that influence the vortices' development, a quasi-Lagrangian approach is adopted in which the budget is evaluated in coordinates following the leading line (see Gao et al. 1990). All terms on the rhs of (1) and (2) have been computed, and then the residual is attributed to the quasi-Lagrangian vorticity tendency, that is, the storage term on the lhs of (2). In the present

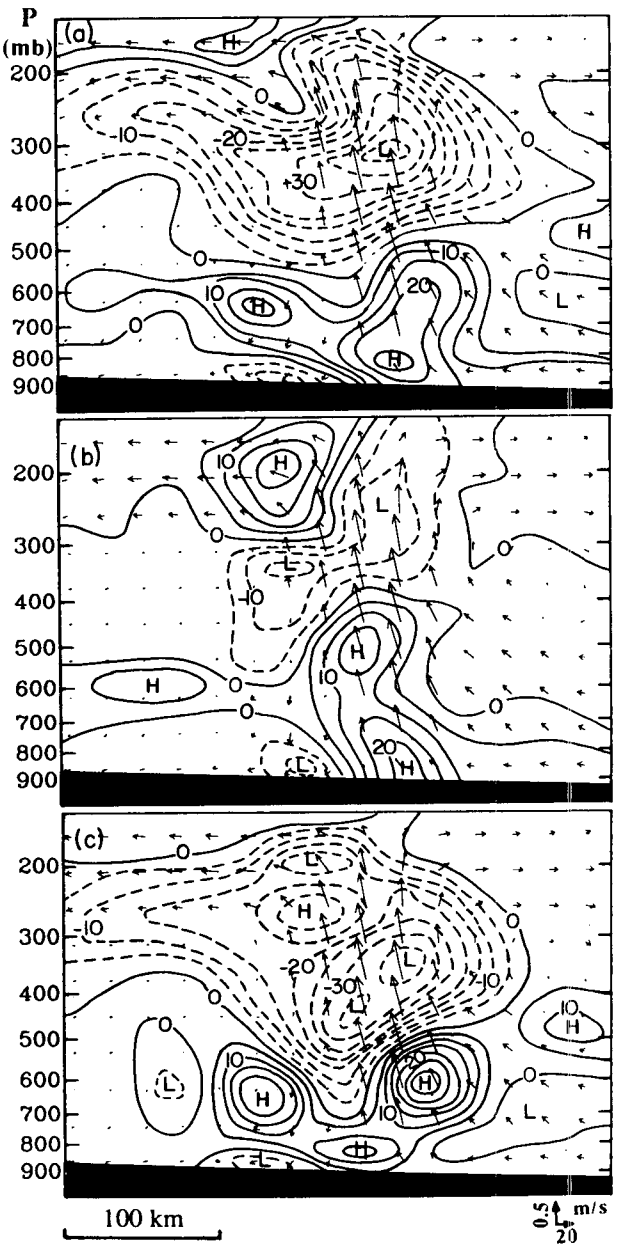

FIG. 11. Vertical cross section of (a) Lagrangian absolute-vorticity tendency $[D(\zeta+f)/Dt]$; (b) vortex stretching $[-(\zeta+f)(\partial u/\partial n + \partial v/\partial s)]$; and (c) tilting of horizontal vorticity $[-(\partial\omega/\partial n)(\partial v/\partial p) - (\partial\omega/\partial s)(\partial u/\partial p)]$ at intervals of 5×10^{-5} s^{-1} h^{-1}, superposed with relative-flow vectors from 12-h simulation, valid at 0000 UTC 11 June 1985. Solid (dashed) lines are positive (negative) tendencies.

case, the only error contained in the storage term is related to the aforementioned boundary-layer effect.

Figure 11 shows vertical cross sections of the Lagrangian absolute-vorticity tendency, the stretching and the tilting contributions, superposed with relative flow vectors during the squall's incipient stage. The Lagrangian tendencies exhibit tremendous anticyclonic production in the upper troposphere and cyclonic production in the lower troposphere, with two positive centers corresponding to the leading and wake vortices, respectively; its maximum spinup rate exceeds 2 $\times 10^{-4}$ s^{-1} h^{-1}. Although strong low-level convergence and upper-level divergence have developed during this rapidly intensifying stage, they are only in phase with the leading updrafts (Fig. 4b). Thus, vortex stretching produces a pronounced cyclonic tendency below and an anticyclonic tendency above along the leading line (Fig. 11b). Even though the FTR and RTF flows cause a secondary convergence center near the level of the wake-vortex core, the resultant stretching term contributes only slightly to the Lagrangian tendency of the wake vortex owing to the relatively small absolute vorticity distributed along the interface. At this time, the wake vortex is located about 100 km behind the interface, which coincides roughly with a favorable convergence region associated with the midlevel short-wave trough (not shown). Therefore, the wake vortex is maintained during this period through the stretching of the absolute vorticity mostly pertaining to the short wave.

While the stretching contribution to the wake vortex is small during the intensifying stage, the tilting of horizontal vorticity produces a marked cyclonic tendency ahead of the wake vortex (Figs. 11a and 11c). Note that the maximum tilting occurs near 650 mb, which is below the core of the wake vortex (cf. Figs. 11c and 4b). This appears to be related to the cooling mechanisms whereby strong downward motion is induced. Specifically, at this time, most of the cooling is associated with melting and evaporative cooling and produced by the rearward descending of the midlevel low-θ_e air from the downshear side of the line (also see Fig. 3 in ZG). Only when the sublimative cooling or stratiform precipitation becomes more significant at a later stage will the levels of maximum descending and tilting be elevated.

To understand how the FTR-ascending and the RTF-descending currents help generate vertical vorticity through tilting, Fig. 12 shows a vertical cross section of the tilting of the across-line vorticity, that is, $-(\partial\omega/\partial n)(\partial v/\partial p)$, superposed with the along-line winds (dotted lines). The flow structure exhibits relatively weak along-line shears ahead of, but strong shears behind, the leading line. The development of such strong along-line shear to the rear, as discussed in Zhang and Cho (1992), is a consequence of slantwise adjustment associated with latent heating in the FTR ascending flow and latent cooling in the RTF descending flow. Specifically, a portion of air mass with negative MPV

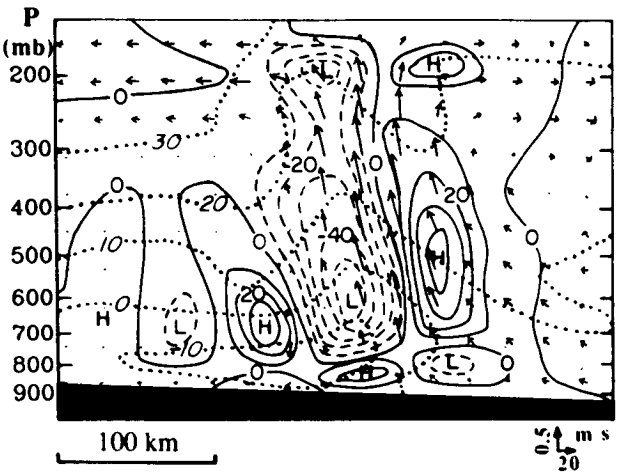

FIG. 12. As in Fig. 11c but for tilting of horizontal across-line vorticity $(-\partial\omega/\partial n)(\partial v/\partial p)$ at intervals of 10^{-4} s^{-1} h^{-1}. The dotted lines are the along-line winds at intervals of 10 m s^{-1}.

(mainly due to convectively unstable conditions) ahead of the leading line was found being transported rearward by the FTR flow, and later stored in the system's wake also with negative MPV, but in a form of across-line baroclinity and strong along-line shear. Given that the winds along the line increase with height as in the present case, the leading updrafts tend to produce a vortex couplet (cyclonic on the right and anticyclonic on the left), whereas the downdrafts to the rear produce an opposite vortex couplet, with the anticyclonic portion superimposed on the vortex couplet to its front. This configuration is similar to that described by BH for the present case, Rotunno (1981) for the development of tornadic storms, and Wilhelmson and Klemp (1978) for storm splitting, but at different scales. It is apparent that the deep and strong anticyclonic vorticity between the leading and wake vortices in Figs. 4b–d is initially generated by upward tilting followed by downward tilting of the horizontal vortex tubes, associated with the vertical shear along the line, and later enhanced by negative stretching along the convergence zone. Note that the tilting of along-line vorticity into vertical vorticity, that is, the term $(\partial\omega/\partial s)(\partial u/\partial p)$, is also significant (cf. Fig. 11c and 12) because of the development of more localized vertical motion during this formative stage. This effect becomes smaller when deep convection is well organized along the leading line, except for the regions near the southern and northern ends of the line. Nevertheless, this term contributes positively to the northward extension of the wake vortex in the stratiform region, and explains partly why a deep cyclonic vortex layer could develop near the northern end of the squall system (see Fig. 5).

By 0300 UTC, the FTR ascending and RTF descending currents in the squall system have fully developed (Fig. 13), as well as the leading vortex and the anticyclonic vorticity along the interface (Fig. 4c).

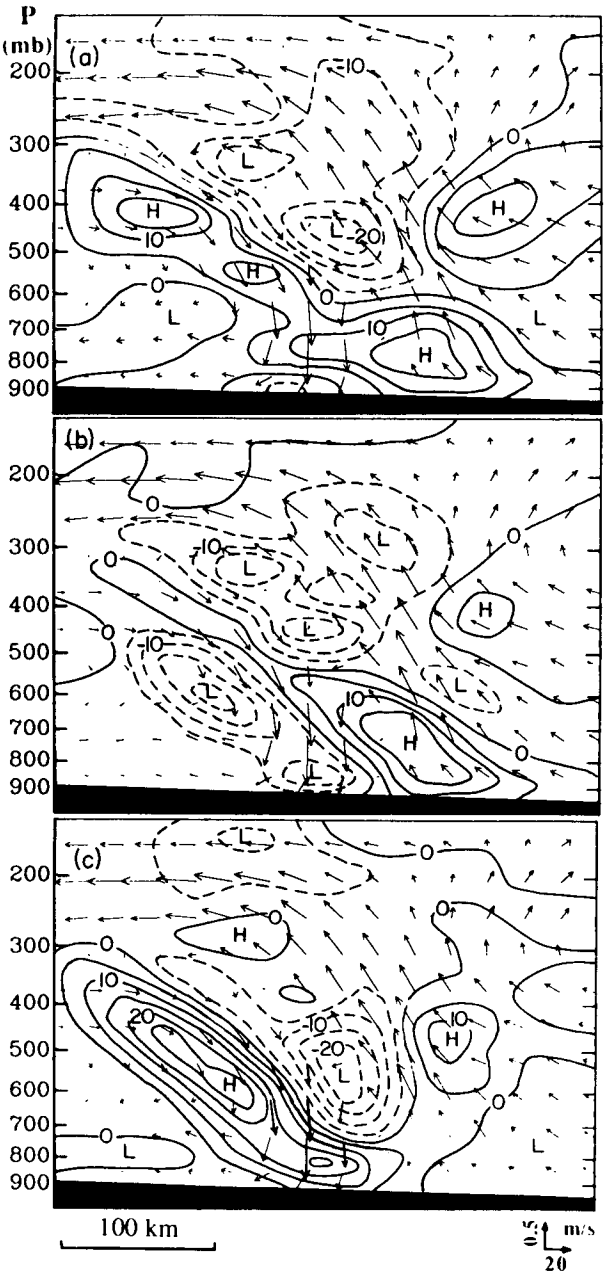

FIG. 13. As in Fig. 11 but from 15-h simulation, valid at 0300 UTC 11 June 1985.

Thus, their pertinent net tendencies are smaller than those that occurred during the rapidly intensifying stage (cf. Figs. 11a and 13a). A deep layer (up to 300 mb) of net cyclonic-vorticity production associated with the wake vortex, however, occurs along the leading edge of descending RTF inflow. This cyclonic-vorticity tendency is produced by weak stretching followed by strong tilting. Of striking significance is that *the contribution from the tilting of horizontal vorticity to the wake vortex by the descending rear inflow is about one order of magnitude larger than that from the stretching.* This finding, to a certain extent, agrees with BH's conclusion; their analysis, however, shows only this significant tilting effect in association with dry rear-inflow subsidence at the back edge of the stratiform region. It is evident that stronger descending motion or stronger mid- to upper-level cooling will intensify the wake vortex through tilting, further revealing that the wake vortex is cooling induced. Notwithstanding its relatively small contribution, the stretching effect has increased along the leading edge of descending flow as a result of the forward acceleration of the wake vortex into the tilted convergence zone along the interface. Nevertheless, because the RTF descending flow is highly divergent (see Figs. 4c and 7), *the stretching effect in most of the RTF flow tends to locally destroy the wake vortex during the system's development stage.* This negative effect offsets a significant fraction of the positive contribution from the tilting in the lower half of the vortex layer. Despite this significant offset, the net Lagrangian tendency still shows that the tilting of horizontal vorticity by the descending flow determines the depth and magnitude of the wake vortex during this stage. It follows that *vortex tilting by the descending RTF flow can create a strong wake vortex without requiring preexisting cyclonic vorticity,* as in the present case, associated with a midlevel meso-α-scale short wave.

From Figs. 11a and 13a, one may note that the center of the Lagrangian cyclonic-vorticity tendency associated with the wake vortex is elevated as the sublimative cooling becomes more dominant. Yet, the core of the wake vortex remains near 550 mb during most periods of the system's life cycle (Fig. 4). Thus, advective processes must play an important role in redistributing the convectively generated vorticity. Figure 14 shows vertical cross sections of the quasi-Lagrangian vorticity tendency ($\delta\zeta/\delta t$), horizontal (relative) vorticity advection across $[-u\partial(\zeta+f)/\partial n]$ and along the line $[-v\partial(\zeta+f)/\partial s]$, and vertical vorticity advection $(-\omega\partial\zeta/\partial p)$ in relation to the squall circulations. It is evident that horizontal advection along the line has the least effect on the redistribution of the vorticity source in the stratiform region (Fig. 14c). The vertical advection in the descending flow tends to reduce the magnitude of cyclonic vorticity in the upper-half portion and increase it in the lower-half portion of the wake vortex (Fig. 14d). Thus, without the continuous strong cyclonic-vorticity supply through the vortex tilting at the upper levels (e.g., near 400 mb, Fig. 13a), the wake vortex would be advected rapidly downward and eventually destroyed in the lower layers by the divergent outflow and friction. The effect of the across-line advection by the RTF flow is to accelerate the wake vortex toward the interface (Fig. 14b). The net result is that the wake vortex gains a cyclonic-vorticity tendency of 8×10^{-5} s^{-1} h^{-1} at its core following the squall system (Fig. 14a). This magnitude is comparable with the simulated growth rate of the wake vortex during the mature to decaying stages (cf. Figs. 4c–d).

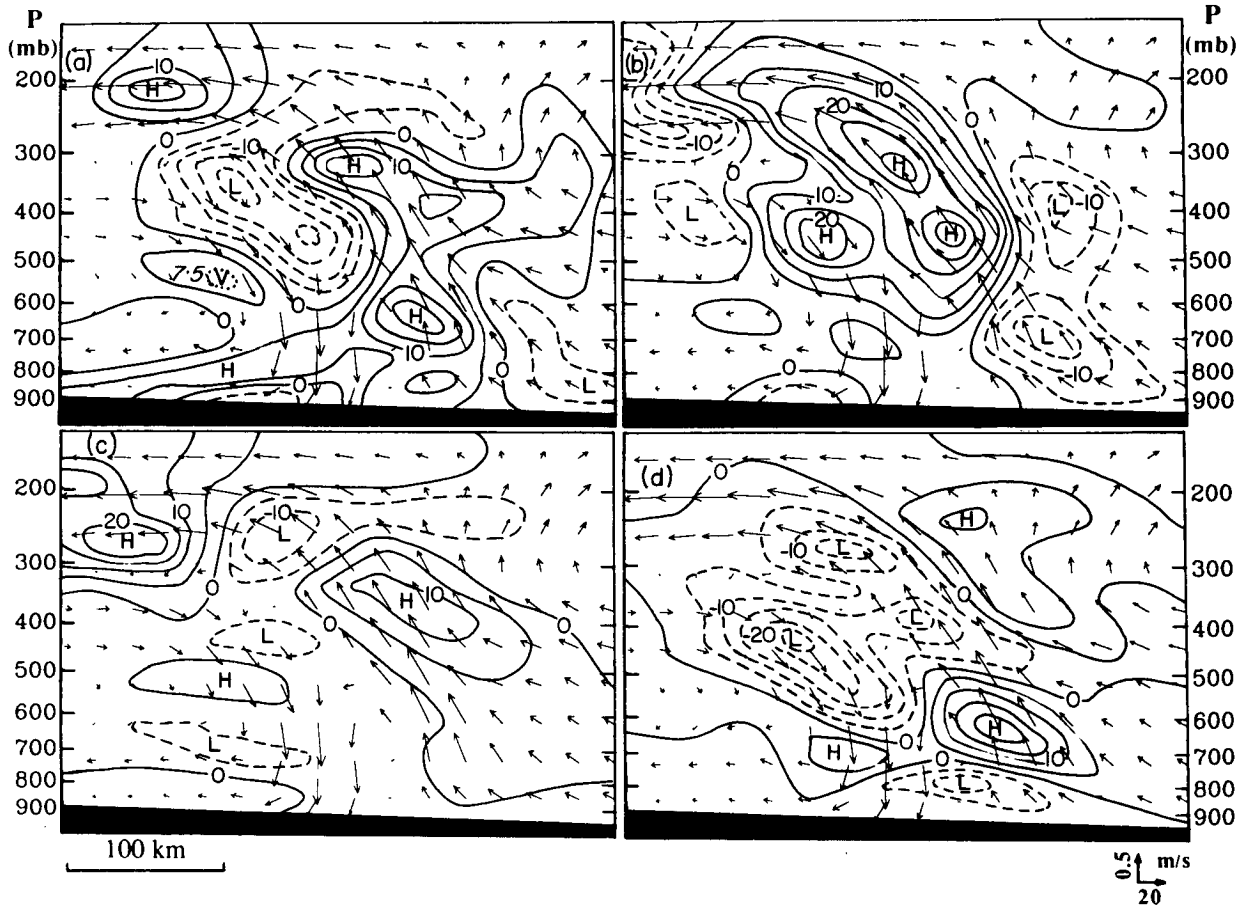

FIG. 14. Vertical cross section of (a) quasi-Lagrangian vorticity tendency ($\delta\zeta/\delta t$); (b) relative horizontal across-line advection [$-u\partial(\zeta+f)/\partial n$]; (c) horizontal along-line advection [$-v\partial(\zeta+f)/\partial s$]; and (d) vertical advection ($-\omega\partial\zeta/\partial p$) at intervals of 5×10^{-5} s^{-1} h^{-1}, superposed with relative flow vectors from 15-h simulation, valid at 0300 UTC 11 June 1985. Solid (dashed) lines are positive (negative) tendencies.

It is worth noting that the relative horizontal advection across the line produces positive vorticity tendencies in the vicinity of the interface where the aforementioned anticyclonic-vorticity zone is located. Thus, the horizontal vorticity advection by the FTR and RTF flows acts, through "horizontal mixing" of positive and negative vorticity, against the anticyclonic-vorticity production by tilting and negative stretching (see Figs. 11b and 13b). This indicates that the midlevel anticyclonic-vorticity structure is a transient feature, which means that this type of anticyclonic vortex will dissipate rapidly once the forcing mechanism vanishes. Its counterparts at the lower and upper levels, however, can survive for a longer period.

As the system enters the dissipating stage around 0600 UTC, the wake vortex propagates into the strong convergence zone along the interface (Fig. 4d). Thus, the stretching of the wake vortex itself gives rise to extremely large concentrations of cyclonic vorticity along the interface (Fig. 15b). This rate considerably overcompensates the negative tilting effect along the interface for the amplification of the wake vortex (Fig. 15a). Note the more upright and symmetric structure of the wake vortex during this stage, as compared to its rearward-tilted distribution when the tilting effect dominates (cf. Figs. 4c,d). The tilting effect changes its role in the intensification of the wake vortex at this time because the vortex advances into the interface where the tilting always generates anticyclonic vorticity. Even behind the wake vortex, the tilting effect is much smaller than that during the formative stage, owing to the weakening of both the shears and descending motion. The net Lagrangian cyclonic-vorticity tendency associated with the wake vortex, located at 500 mb, exceeds 45×10^{-5} s^{-1} h^{-1}, which is much greater than ever occurred during the formative stage. This further reveals that this type of mesovortex has better-defined circulation characteristics during the decaying stage of MCSs. Nevertheless, in the lower-half portion of the vortex layer, the stretching associated with the divergent outflow again tends to destroy the wake vortex locally. Hence, the roles of the vortex stretching are to enhance

the upper portion, but to weaken the lower portion of the wake vortex. Then, the descending rear inflow advects the cyclonic-vorticity surplus in the upper layers downward to make up the vorticity deficit in the lower layers, such that the wake vortex is maintained within a deep layer.

It is extremely important to point out that the amplification of the wake vortex as the system decays by no means implies that the system's dissipation has positive or no effects on the intensity of the vortex. Rather, it reflects the increasing importance of the stretching as the wake vortex approaches the convergence zone along the interface. In fact, as the FTR ascending flow weakens, the convergence along the interface decreases rapidly because of less latent heat release occurring in the FTR ascending flow and less condensate available for subsequent diabatic cooling in the stratiform region (see ZG for more details). Thus, by 0800 UTC, the wake vortex has weakened from its peak intensity (which occurred roughly between 0630 and 0700 UTC) and its core has shifted from 550 to 650 mb after the upper-level vorticity sources diminished (see Fig. 6). The dominant role of the vortex stretching in cyclonic-vorticity generation suggests that quasigeostrophic theory could be used to *partly* explain the development and subsequent maintenance of the wake vortex near the end of the squall's life cycle (i.e., after 0800 UTC in this case). This can be seen from Fig. 3 in ZG and Figs. 8–10 herein that the wake vortex may reach a quasi-balanced state with the short-wave trough during this stage.

Figure 15 also contains additional information on the rapid dissipation of the anticyclonic vorticity centered along the interface (cf. Figs. 4b–d). As previously mentioned, the tilting of horizontal vorticity always favors the generation of anticyclonic vorticity between peak ascent and peak descent, provided that the along-line winds increase with height. As the wake vortex propagates into the convergence zone, however, the anticyclonic-vorticity production by tilting becomes overcompensated by the stretching of the wake vortex itself (Fig. 15a). Thus, the resulting net Lagrangian tendency can destroy the anticyclonic vorticity at a time scale of about 1 h, assuming a moderate rate of $20 \times 10^{-5}\ s^{-1}\ h^{-1}$. With additional contribution from the horizontal vorticity advection by the FTR and RTF flows, this dissipation time scale could be further reduced. Nevertheless, the horizontal "mixing" should be considered as the primary cause for the dissipation of the anticyclonic-vorticity zone.

Finally, Figs. 16 and 17 show the horizontal distribution of the vorticity-budget terms at 600 mb during the mature stage and at 500 mb during the decaying stage, respectively, in order to demonstrate that the aforementioned vorticity-budget results are representative of the entire squall system. At 0300 UTC, the significant vorticity sources or sinks are distributed over the northern portion of the squall system. Tilting of

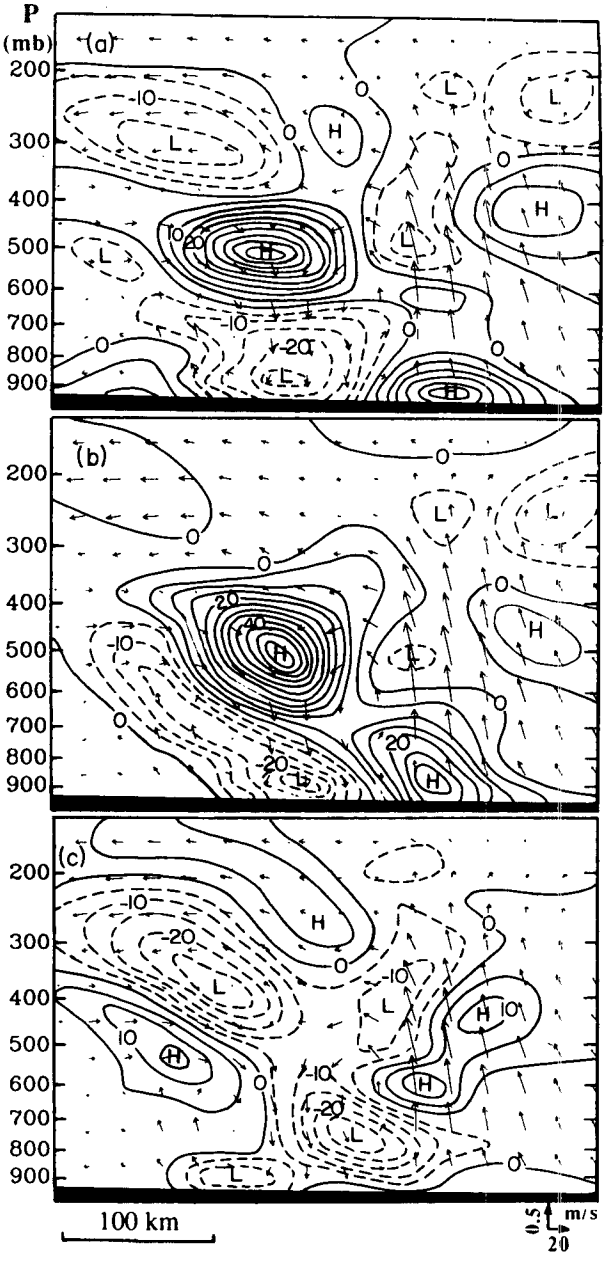

FIG. 15. As in Fig. 11 but from 18-h simulation, valid at 0600 UTC 11 June 1985.

horizontal vorticity behind the flow interface basically determines the intensity of the wake vortex (Figs. 16a,c). Tilting also appears to be responsible for the northeast–southwest elongation of the vortex during this period. On the other hand, vortex stretching is more or less a sink to the wake vortex in the low-to-mid levels owing to the divergent descending flow (see Figs. 13b and 16b), even though an elongated region of midlevel convergence has developed behind the leading line (see Fig. 1b).

As the wake vortex comes into phase with the RTF–

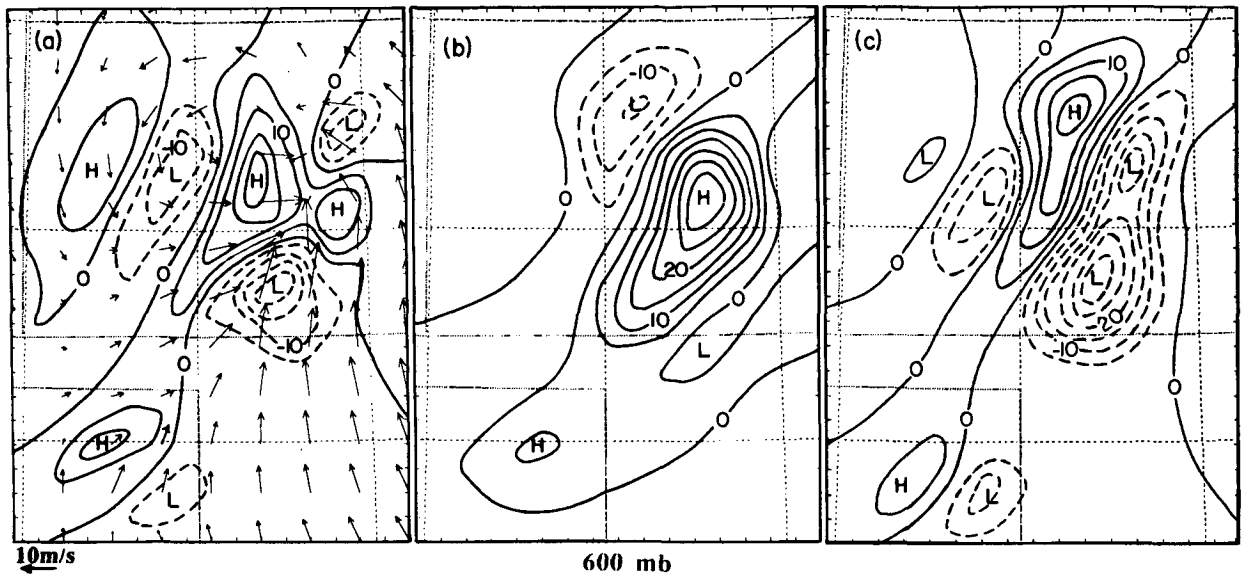

FIG. 16. Horizontal distribution of (a) Lagrangian absolute-vorticity tendency $[D(\zeta+f)/Dt]$; (b) vortex stretching $[-(\zeta+f)(\partial u/\partial n + \partial v/\partial s)]$; and (c) tilting of horizontal vorticity $[-(\partial\omega/\partial n)(\partial v/\partial p) - (\partial\omega/\partial s)(\partial u/\partial p)]$ at intervals of 5×10^{-5} s^{-1} h^{-1}, superposed with relative-flow vectors at 600 mb from 15-h simulation, valid at 0300 UTC 11 June 1985. Solid (dashed) lines are positive (negative) tendencies.

FTR flow interface, however, vortex stretching plays a much more important role than the tilting effect in further spinning up the vortex (Fig. 17). As Fig. 17b shows, an elongated region of strong vortex stretching, with its maximum occurring at 500 mb (also see Fig. 5), is rather uniformly distributed along the interface, though some variabilities along the line are still notable. Thus, the wake vortex rapidly expands into the entire stratiform region, resulting in a much larger-scale wind circulation (see Fig. 1c). It is also evident that the vortex stretching overcompensates the negative tilting effect along the interface, leading to the rapid collapse of the anticyclonic vorticity in the region.

6. Discussion and speculations

From the present study and the BH composite analysis, the convectively generated 2D vorticity structure of the 10–11 June 1985 squall system during the mature stage is characterized by a deep cyclonic vortex along

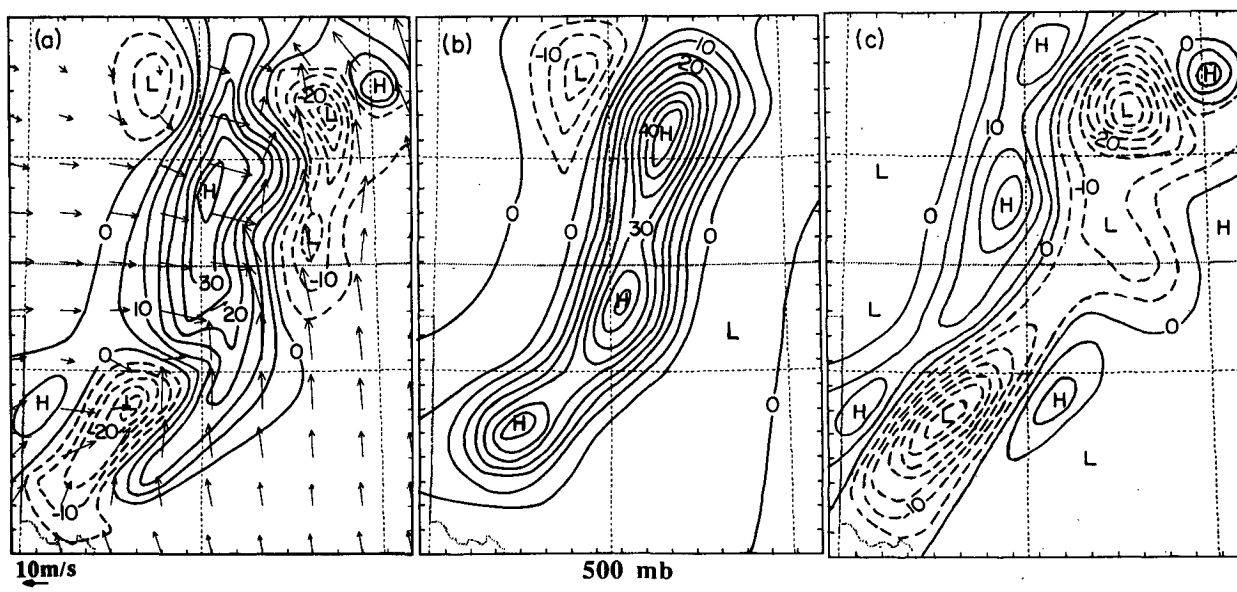

FIG. 17. As in Fig. 16 but at 500 mb from 18-h simulation, valid at 0600 UTC 11 June 1985.

the leading line and by a midlevel mesovortex in the stratiform region with an intermediate anticyclonic-vorticity zone. These vortices are produced either by latent heating or by cooling through tilting and stretching at different scales. Since the present squall line contains many classical squall-line characteristics (e.g., a midlevel short wave, FTR updrafts, RTF descending flow, trailing stratiform clouds, and surface pressure highs and lows), the vorticity structures, evolution, and processes that lead to the mesocyclogeneses may be common to other midlatitude squall lines that are trailed by stratiform precipitation. Perhaps the evolution and the intensification mechanisms of vortices presented herein are more "complicated" than what previous observational studies have indicated. This is because most previous studies have captured only a particular stage of an MCS life cycle (e.g., the mature stage by BH; the decaying stage by Stirling and Wakimoto 1989, Verlinde and Cotton 1990, Bartels and Maddox 1991, and Johnson and Bartels 1992). Furthermore, the use of any composite techniques would often fail to reveal certain important internal structures. Therefore, obtaining high-resolution observations for an entire MCS life cycle in future field experiments is extremely important in order to avoid some undue conclusions on the development of the meso-β-scale structure and evolution of MCS's. Furthermore, the rawinsonde observations during PRE-STORM are still too coarse to resolve the detailed structure of mesovortices. Other important implications of the present study are discussed below.

a. Genesis of a cooling-induced mesovortex

Numerical sensitivity experiments with the present case, as given in ZG, show that the RTF descending flow does not extend downward to the surface and wake lows fail to develop when either ice microphysics or resolvable-scale evaporative cooling is turned off (see their Figs. 12–17). Moreover, the model tends to generate an excessively strong and deep cyclonic circulation to the northern side of the line. This further reveals that sublimative and evaporative cooling is instrumental in the development of the descending rear inflow and the wake vortex. In this study, we have shown that tilting of across-line vorticity dominates the *early* development of the wake vortex and that vortex stretching determines the *final* intensity of the wake vortex. Evidently, stronger upper-level cooling would more likely result in a more pronounced wake vortex through both tilting and stretching. During the decaying stage, stronger latent heating in the FTR ascending flow would also assist the intensification of the wake vortex through stretching along the flow interface.

The vorticity budget presented in section 5 indicates that the tilting alone could rapidly create a strong midlevel vortex without requiring *preexisting* relative vorticity, and then, its further spinup can be substantially strengthened by stretching. In the present case, the convectively generated portion of the wake vortex is more than five times larger than the initial relative vorticity associated with a meso-α-scale short wave. Thus, it becomes apparent that if these vorticity sources act locally in the stratiform region owing to the presence of mid- to upper-level cooling, varying scales of midlevel mesovortices could be produced, which depend upon the scale of the vorticity sources. In nature, a squall system may consist of numerous "supercells" along the leading line and several centers of vertical motion in the stratiform region, which could clearly lead to the development of multiple mesovortices. This implies that the multiple mesovortices shown in Smull and Houze (1985), Stirling and Wakimoto (1989), and Verlinde and Cotton (1990) may be produced directly by localized vorticity sources rather than by the splitting of a larger-scale vortex or the upward momentum transport by multiple convective updrafts. The results also explain why different scales of midlevel mesovortices could be generated, as have recently been reported.

It should be noted, though, that the tilting effects on the generation of wake vortices depend on the wind shears in the stratiform region rather than on the squall's environment. This implies that strong wake vortices could be created in the trailing stratiform region of a midlatitude squall line even in a weak-shear environment, since convective and mesoscale updrafts and downdrafts will redistribute horizontal momenta vertically and may also generate strong vertical shears to the rear of the system. Zhang and Cho (1992) have discussed how strong vertical shears along the line can be convectively generated under weak-shear conditions, based simply on the absolute momentum conservation principle in a 2D framework. Specifically, as the RTF (FTR) flow descends (ascends), the change in flow velocity should mostly occur in the direction parallel to the squall line; this change amounts to the product of the local Coriolis parameter and the distance traveled by air parcels in the direction across the line. Therefore, an air parcel following the FTR ascending (RTF descending) flow will gain (lose) along-line momentum by 10 m s^{-1} for every 100-km across-line displacement, assuming $f = 10^{-4}$ s^{-1}. Of course, in a 3D framework the resulting vertical shear in the trailing stratiform region will be affected by the convectively generated pressure gradient along the line. A more comprehensive understanding of these dynamic processes based on the MPV conservation constraints has also been provided by Zhang and Cho (1992).

b. Different types of midlevel mesovortices

If the present results are synthesized with previous studies of mesovortices, there seem to be two types of midlevel mesovortices that can be generated in the trailing stratiform region of MCS's: the first type, often

referred to as the warm-core mesovortex, is induced by low- to midlevel latent heating, and develops in mesoscale ascent (Bosart and Sanders 1981; Zhang and Fritsch 1987, 1988b; Kuo et al. 1988; Menard and Fritsch 1989); the second type is induced by mid- to upper-level latent cooling, and develops in mesoscale descent, as the present wake vortex and that in Brandes (1990) and Johnson and Batels (1992). Zhang and Fritsch (1987; 1988a,b) have provided extensive discussions on the formation of warm-core vortices in mesoscale ascending flow. Although parts of their discussions can be applied to cooling-induced vortices, there are a number of differences in the basic structure and formative mechanisms that need clarification. Specifically, for the heating-induced vortices, a midlevel warm-core structure can be expected when the latent heating exceeds upward adiabatic cooling. Then, a cyclonic circulation will be produced below the warmest air primarily through stretching (Zhang and Fritsch 1987; Chen 1990). A long-lived warm-core structure requires that diabatic heating occur at a scale comparable to, or larger than, the Rossby radius of deformation, such that most of the heating goes into the quasi-balanced flow (Ooyama 1982; Frank 1983; Cotton et al. 1989). Later, the vortex circulation is maintained through the thermal-wind relationship. In contrast, since cooling-induced vortices intensify in descending motion, mid- to upper-level diabatic cooling associated with stratiform precipitation is responsible for the spinup of cyclonic vorticity, initially through the tilting of horizontal vorticity, and later enhanced by the vortex stretching. Because the maximum cooling occurs near the core of wake vortices, the thermal-wind relationship cannot be utilized to explain the development of wake vortices. Therefore, unlike warm-core vortices in which the planetary vorticity plays an important role in geostrophically adjusting atmospheric flow to the warm-core structure, *the earlier development of wake vortices does not require the planetary vorticity.* They could even develop near the equator as long as vertical shears can be induced behind the convective line as a result of vertical momentum transport, mid- to upper-level cooling, and descending motion. This is more likely the mechanism whereby tropical mesovortices, such as those analyzed by Zipser (1969), Houze (1977), and Gamache and Houze (1982), develop in squall systems that are trailed by stratiform precipitation.

Warm-core mesovortices are often characterized by convergence attended by cyclonic vorticity in the lower troposphere, and divergence accompanied by anticyclonic vorticity in the upper troposphere (Zhang and Fritsch 1987, 1988b; Kuo et al. 1988; Chen 1990). Thus, mesoscale circulations from the low to upper levels within MCS's are well coupled through mesoscale updrafts. In addition, Zhang and Cho (1992) found that the often-observed upper-level divergence and anticyclonic vorticity are a consequence of upward transport of negative MPV from the convectively unstable boundary layer ahead of MCS's. In this respect, warm-core vortices may play an important role in the organization of MCS's (Zhang and Fritsch 1987), and thus intensify with the same pace as their parent MCS's.

On the other hand, cooling-induced vortices tend to decouple from ascending currents above the RTF and FTR flow interface during the system's intensifying stage, even though they exhibit a closed circulation in a horizontal plane (see footnote 2). The role of wake mesovortices, through their descending RTF flow components, is to provide a source of dry air that enhances sublimative and evaporative cooling and to maintain a cold pool within the stratiform region. These processes can either help sustain MCS's if the convectively generated along-line vorticity roughly balances the pertinent cold pool circulation (Rotunno et al. 1988) or accelerate the demise of MCS's when they advance into convectively less favorable environments (ZG). Because the most rapid intensification of cooling-induced vortices occurs when they become in phase with major convergence zones, their structures are better developed during the decaying stage of MCS's. Moreover, at this stage, both latent cooling in RTF descending flow and latent heating in FTR ascending flow contribute directly to the amplification of wake vortices, that is, due to the presence of convergence.

Warm-core mesovortices often exhibit a deep layer of warm air overlying a pool of cold, moist air in the lowest layers during the mature stage. By comparison, cooling-induced vortices are characterized by a deep, divergent outflow in the lower troposphere with a cold, moist anomaly in the upper portion and a warm, dry anomaly in the lower portion of the vortex circulations. Only the midlevel convergence, which occurs in phase with the vorticity concentration, can make a positive contribution to the spinup of the vortices. Furthermore, in a weak-gradient environment, the midlevel warm-core structure is in a more balanced state with horizontal winds, whereas the midlevel cold anomaly tends to be unbalanced, and it merely can occur at the precipitation scales.

Having discussed various differences in the vortex properties, it is natural at this point to infer what environmental conditions are favorable for the development of cooling- versus warming-induced mesovortices. The present study shows that strong sublimative and evaporative cooling is essential in the intensification of cooling-induced vortices. Hence, the presence of a dry midtroposphere and a moist lower troposphere in combination with baroclinically induced larger-scale midlevel relative rear inflow would assist the generation of cooling-induced mesovortices. Conversely, warm-core mesovortices favor a relatively weaker-gradient environment with a deep layer of moist air in the low- to midtroposphere, which is similar to that described by Maddox (1980; 1983) for MCCs. Then, the rear

inflow of cold, dry air and the subsequent diabatic cooling and cold outflow will be relatively weak; the system may move slowly. The slowly moving MCS's would also be less likely to spawn strong cooling-induced vortices owing to the convective moistening of the troposphere to the rear. The presence of a low-level jet tends to enhance the cyclonic-vorticity production for the spinup of warm-core vortices. Furthermore, because of the weak-gradient environment, there is no well-defined relationship between the larger-scale forcing and the evolution of deep convection. It is possible, then, that the preexisting cyclonic circulation associated with a short-wave trough can synergize with latent heat release to assist its further concentration of cyclonic vorticity.

As previously mentioned, the present wake vortex originates from and later evolves within a midlevel short-wave trough. One sensitivity experiment, in which all diabatic forcings were turned off, shows that at 18-h simulation, the midlevel traveling short wave is almost indiscernible above 700 mb, and, as with the surface front (see Fig. 18 in ZG), it lags about 300 km behind that in the control simulation (not shown). This indicates that the diabatic heating in ascending regions tends to enhance the amplitude of the short-wave disturbance, while the cooling in descending regions helps speed up the movement of the short wave. At the end of the system's life cycle, the wake vortex may reach a quasi-balanced state with the mesotrough and become long lived. This aspect will be investigated in a future study in which the present model integration is extended for another 24 h. On the other hand, for warm-core mesovortices, they often develop near a meso-α-scale short-wave trough that is superposed on a large-scale ridge system (e.g., Maddox 1983; Bosart and Sanders 1981). The development of warm-core vortices tends to enhance the short-wave trough by providing more heating in the upper portion of the troposphere (Zhang and Fritsch 1988a). Later, the vortex circulation will be balanced by the warm-core anomaly, and becomes inertially stable if the larger-scale flow deformation is weak (Zhang and Fritsch 1987; 1988a,b).

c. *Relationship between cooling- and heating-induced mesovortices*

While cooling-induced vortices are convectively generated in the descending portion of MCS's, their pertinent characteristics of midlevel convergence and cold anomaly will quickly diminish once the cooling mechanisms vanish. Later, the midlevel mesovortices can become inertially stable under weak-shear environments, as previously mentioned. If the environment into which they propagate is convectively favorable, it is possible that the existing cyclonic circulation could assist the organization of deep convection. Then, mesoscale ascent may dominate over the vortex region, a warm anomaly would likely develop near the core of the vortex, and the warm-core type of vortex circulation would ensue. The key to the relationship between the cooling-induced vortices and subsequent development of a warm-core type of vortex may depend upon whether or not the former could propagate in phase with midlevel mesolow or mesotrough after dissipation of their parent MCS's. Hence, attempts should be made in future field experiments to obtain information on the downstream propagation of midlevel mesovortices and subsequent initiation of deep convection in the vicinity of mesovortices. Nevertheless, in the present case, JH mentioned that rapid surface cyclogenesis occurred as the dissipated squall system moved into the Ohio Valley.

There have been recent observations that some MCS's, which are initiated at the downwind side of the Rocky Mountains, undergo several cycles of development and decay as they propagate over a large distance ($>10^3$ km) over periods of several days (e.g., Bosart and Sanders 1981; Wetzel et al. 1983; Maddox et al. 1986; Murphy and Fritsch 1989). In some instances, these long-lived systems move over warm ocean water and develop into tropical storms (Bosart and Sanders 1981; Velasco and Fritsch 1987). Detailed examination of those systems often reveals the existence of a cyclonic circulation in conjunction with a midlevel meso-α-scale short wave. Therefore, it appears that immediately downstream of a high plateau, such as the Great Plains of the United States, is a favored region for the development of cooling-induced mesovortices, because of the topographically generated dry air that is often elevated above a south-to-southeasterly moist current (see Carlson et al. 1983). Farther to the east, however, a deep layer of moist air is often present in prestorm environments, and the initiation of MCS's is usually accompanied by the development of a low-level jet (e.g., Means 1944). Thus, a warm-core type of mesovortex would likely occur within MCS's in this region.

7. Summary and conclusions

In this study, the structure and evolution of a cooling-induced midlevel mesovortex, referred to as the wake vortex, that developed in the descending rear inflow of the 10–11 June 1985 squall line has been examined, primarily based upon a 20-h real-data simulation of the case. The model simulation has been verified extensively against all available observations in previous studies. The existence of the wake vortex conforms to rawinsonde observations and dual-Doppler radar analysis, but its midlevel cooling structure has not been revealed by previous studies, undoubtedly owing to its relatively small horizontal scale. The present midlevel mesovortex originates from the pre-existing cyclonic vorticity associated with a meso-α-scale short wave. It is initially maintained through the ver-

tical stretching of its absolute vorticity pertinent to the short wave. Later, when the squall system becomes well organized, the larger-scale RTF relative inflow of dry and cold air plus the rearward descending of lower-θ_e air from the downshear side of the squall line cause pronounced cooling by sublimation, melting, and evaporation in the stratiform region, thereby leading to the rapid development of descending rear inflow and vertical shears behind the leading line. Then, the descending motion coupled with the positive along-line shear enhances the pre-existing vortex circulation through tilting of the horizontal vorticity. It is found that the tilting effect is about one order of magnitude larger than the stretching effect during the intensifying stage. In most vortex layers, the stretching even tends to locally destroy the vortex due to the presence of divergent outflow in the lower troposphere. As the wake vortex is moved by the relative rear inflow into the flow interface, however, the stretching effect dominates the cyclonic-vorticity production, whereas the tilting plays a negative part in the amplification of the vortex.

Figure 18 provides a conceptual model showing the 2D structure of relative vertical vorticity in association with the across-line circulations during the mature stage of the 10–11 June 1985 squall system. A deep layer of strong cyclonic vorticity, referred to as the leading vortex, is generated along the leading convective line (about 70 km wide in the present case), owing to the concurrent positive contributions of tilting and stretching. This vortex is warm cored and extends to the trailing stratiform region. In a certain sense, the warm-core vortex plays an important role in organizing mesoscale flows from the lower to upper troposphere through convective and FTR mesoscale updrafts. Based on the conservation of MPV, anticyclonic vorticity should be expected in the upper portion of overturning updrafts after air parcels from the convectively unstable boundary layer have passed their equilibrium levels in the upper troposphere. Similarly, another local maximum of anticyclonic vorticity should appear to the rear of the stratiform precipitation region. This anticyclonic vorticity also extends to mid-to-lower levels along the interface, owing to tilting of horizontal vorticity by the FTR ascending and RTF descending flows and later to negative stretching in the convergence zone. The wake vortex develops in the descending rear inflow beneath the active stratiform cloudiness, with its maximum intensity occurring above the melting level. The wake vortex has a scale of 120–150 km in its across-line dimension, but its longitudinal dimension during the decaying stage is more than 300 km. There is a constant-θ_e surface situated along the flow interface that acts to separate the FTR from the RFT flow. Thus, the wake vortex decouples from the upper-level FTR ascending and anticyclonic flow during this formative stage. At the surface, a wake depression tends to develop as an end product of the development of stratiform precipitation, descending rear inflow and the wake vortex.

As the squall system enters its decaying stage, the above conceptual model needs to be substantially modified. Specifically, the wake vortex is advected into the flow interface and comes into phase with the major convergence zone, thus causing the rapid spinup of the midlevel vortex through stretching. In contrast, because deep convection along the leading line dissipates, the leading vortex rapidly decays, shrinking in both depth and width, and eventually merging into the wake vor-

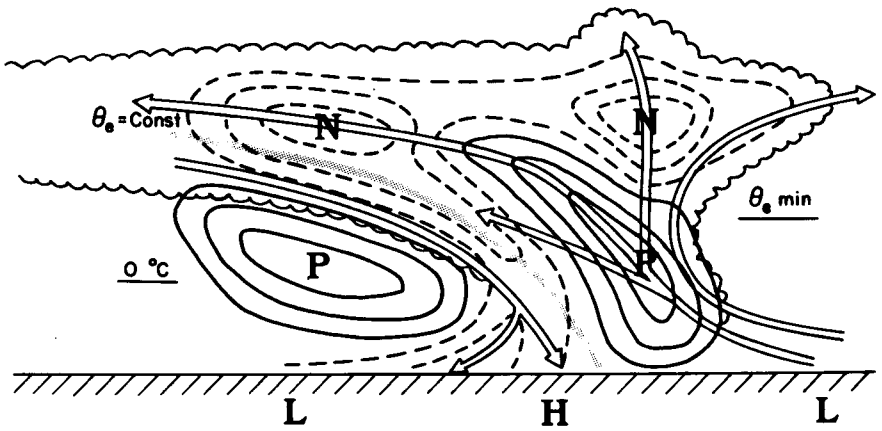

FIG. 18. The 2D conceptual distribution of relative vertical vorticity in a cross section taken normal to the leading convective line during the mature stage of the 10–11 June 1985 squall system. Solid (dashed) lines denote relative cyclonic (anticyclonic) vorticity, with its local maxima represented by the letter, P (N). Open arrows indicate the internal circulations (e.g., overturning updrafts, FTR updrafts, and overturning downdrafts) of the squall system. A shaded line is used to represent the FTR and RTF flow interface. The letters H and L denote the surface mesohigh and mesolow pressure centers, respectively.

tex. The midlevel anticyclonic-vorticity zone also rapidly dissipates, primarily owing to the horizontal vorticity "mixing" by the FTR and RTF flows. At the end of the life cycle, the wake vortex becomes the only remaining element of the internal squall-line circulations that can be observed in a deep layer and at a larger scale in the low to midtroposphere.

It is necessary to emphasize that the wake vortex and the squall's circulations are 3D in character and should be visualized in a 3D framework. In particular, the present wake vortex tilts northward with height so that the pertinent cyclonic vorticity occupies most of the troposphere near the northern end of the system during the decaying stage. The main findings of the present study may be summarized as 1) a midlevel mesovortex can develop in the descending rear inflow of an MCS as a result of the mid- to upper-level cooling in the stratiform region; 2) unlike a warm-core mesovortex, the cooling-induced vortex tends to decouple from mesoscale circulations above the flow interface during the system's intensifying stage; 3) tilting and stretching play different roles in the evolution of the vortex during different stages of the system's life cycle; and 4) an anticyclonic-vorticity zone tends to develop behind the leading convective line mostly through tilting and later dissipates mainly due to horizontal "mixing" of vertical vorticity.

In conclusion, we may state that midlevel mesovortices, large or small, strong or weak, deep or shallow, are ubiquitous in MCS's, since they can be induced by either latent heating or cooling; their pertinent mesoscale rotational flow may be one of the basic dynamic effects of MCS's on their larger-scale environments. The longevity and subsequent evolution of mesovortices may be determined by the kinematic and thermodynamic conditions of environmental flow within which they are embedded. The results suggest that vertical (or potential) vorticity should be considered as a fundamental variable to diagnose the structure and evolution of MCS's, because vorticity is a more persistent variable in the atmospheric flow. Finally, the present modeling results pose a serious challenge for future field experiments to obtain 4D high-resolution datasets for a life cycle of MCS's, and for mesoscale analysts to correctly attain the internal structure of MCS's, if scientific understanding of MCS's is to continue to advance.

Acknowledgments. The author is very grateful to Drs. R. A. Houze, J. M. Brown, E. A. Brandes, and an anonymous reviewer for their critical comments, and to Drs. J. M. Fritsch, R. H. Johnson, B. F. Smull, M. I. Biggerstaff, E. J. Zipser, and D. J. Raymond for their helpful discussions. Thanks are also extended to Kun Gao for his assistance in preparing the hourly model output for the present study, and to Ms. U. Seidenfuss for her work on the graphics. The model integration was performed on CRAY X-MP of the National Center for Atmospheric Research, which is sponsored by the National Science Foundation. The research was partly supported by the Natural Science and Engineering Research Council and Atmospheric Environmental Service of Canada.

REFERENCES

Anthes, R. A., E.-Y. Hsie, and Y.-H. Kuo, 1987: Description of the Penn State/NCAR mesoscale model version 4 (MM4). Tech. Note, NCAR/TN-282, 66 pp.

Augustine, J. A., and E. J. Zipser, 1987: The use of wind profilers in a mesoscale experiment. *Bull. Amer. Meteor. Soc.*, **68,** 4–17.

Bartels, D. L., and R. A. Maddox, 1991: Midlevel cyclonic vortices generated by mesoscale convective systems. *Mon. Wea. Rev.*, **119,** 104–118.

Biggerstaff, M. I., and R. A. Houze, Jr., 1991a: Kinematic and precipitation structure of the 10–11 June 1985 squall line. *Mon. Wea. Rev.*, **119,** 3034–3065.

——, and ——, 1991b: Midlevel vorticity structure of the 10–11 June 1985 squall line. *Mon. Wea. Rev.*, **119,** 3066–3079.

Bosart, L. F., and F. Sanders, 1981: The Johnstown flood of July 1977: A long-lived convective storm. *J. Atmos. Sci.*, **38,** 1616–1642.

Brandes, E. A., 1990: Evolution and structure of the 6–7 May 1985 mesoscale convective system and associated vortex. *Mon. Wea. Rev.*, **118,** 109–127.

Carlson, T. N., S. G. Benjamin, G. S. Forbes, and Y.-F. Li, 1983: Elevated mixed layers in the regional severe storm environment: Conceptual model and case studies. *Mon. Wea. Rev.*, **111,** 1453–1473.

Chen, S., 1990: A numerical study of the genesis of extratropical convective mesovortices. Doctoral thesis, The Pennsylvania State University, 178 pp.

Cotton, W. R., M.-S. Lin, R. L. McAnelly, and C. J. Tremback, 1989: A composite model of mesoscale convective complexes. *Mon. Wea. Rev.*, **117,** 765–783.

Cunning, J. B., 1986: The Oklahoma–Kansas preliminary regional experiment for STORM-Central. *Bull. Amer. Meteor. Soc.*, **67,** 1478–1486.

Frank, W. M., 1983: The cumulus parameterization problems. *Mon. Wea. Rev.*, **111,** 1859–1871.

Fritsch, J. M., and C. F. Chappell, 1980: Numerical prediction of convectively driven mesoscale pressure systems. Part I: Convective parameterization. *J. Atmos. Sci.*, **37,** 1722–1733.

Gamache, J. F., and R. A. Houze, Jr., 1982: Mesoscale air motions associated with a tropical squall line. *Mon. Wea. Rev.*, **110,** 118–135.

Gao, K., D.-L. Zhang, M. W. Moncrieff, and H.-R. Cho, 1990: Mesoscale momentum budget in a midlatitude squall line: A numerical case study. *Mon. Wea. Rev.*, **118,** 1011–1028.

Houze, R. A., Jr., 1977: Structure and dynamics of a tropical squall-line system. *Mon. Wea. Rev.*, **105,** 1540–1567.

——, S. A. Rutledge, M. I. Biggerstaff, and B. F. Smull, 1989: Interpretation of Doppler weather-radar displays of midlatitude mesoscale convective systems. *Bull. Amer. Meteor. Soc.*, **70,** 608–619.

Johnson, R. H., and P. J. Hamilton, 1988: The relationship of surface pressure features to the precipitation and air flow structure of an intense midlatitude squall line. *Mon. Wea. Rev.*, **116,** 1444–1472.

——, and D. L. Bartels, 1992: Circulations associated with a mature-to-decaying midlatitude mesoscale convective system. Part II: Upper-level features. *Mon. Wea. Rev.*, **120,** 1301–1320.

——, S. Chen, and J. J. Toth, 1989: Circulations associated with a mature-to-decaying midlatitude mesoscale convective system. Part I: Surface features—Heat bursts and mesolow development. *Mon. Wea. Rev.*, **117,** 942–959.

Johnston, E. C., 1981: Mesoscale vorticity centers induced by mesoscale convective complexes. M.S. thesis, University of Wisconsin, 54 pp.

Kuo, Y.-H., L. Cheng, and J.-W. Bao, 1988: Numerical simulation of the 1981 Sichuan flood. Part I: Evolution of a mesoscale southwest vortex. *Mon. Wea. Rev.*, **116,** 2481–2504.

Lafore, J. P., and M. W. Moncrieff, 1989: A numerical investigation of the organization and interaction of the convective and stratiform regions of tropical squall lines. *J. Atmos. Sci.*, **46,** 521–544.

Leary, C. A., and E. N. Rappaport, 1987: The life cycle and internal structure of a mesoscale convective complex. *Mon. Wea. Rev.*, **115,** 1503–1527.

Maddox, R. A., 1980: Mesoscale convective complexes. *Bull. Amer. Meteor. Soc.*, **61,** 1374–1387.

——, 1983: Large-scale meteorological conditions associated with midlatitude, mesoscale convective complexes. *Mon. Wea. Rev.*, **111,** 1475–1493.

——, K. W. Howard, D. L. Bartels, and D. M. Rodgers, 1986: Mesoscale convective complexes in the middle latitudes. *Mesoscale Meteorology and Forecasting,* P. Ray, Ed., Amer. Meteor. Soc., 390–413.

Means, L. L., 1944: The nocturnal maximum occurrence of thunderstorms in the midwestern states. Report No. 16, University of Chicago, 38 pp.

Menard, R. D., and J. M. Fritsch, 1989: A mesoscale convective complex-generated inertially stable warm core vortex. *Mon. Wea. Rev.*, **117,** 1237–1261.

Murphy, J. D., and J. M. Fritsch, 1989: Multiple production of mesoscale convective systems by a convectively-generated mesoscale vortex. Preprints, *12th Conf. on Weather Forecasting and Analysis,* Monterey, CA, Amer. Meteor. Soc., 68–73.

Ogura, Y., and M.-T. Liou, 1980: The structure of a midlatitude squall line: A case study. *J. Atmos. Sci.*, **37,** 553–567.

Ooyama, K., 1982: Conceptual evolution of the theory and modeling of the tropical cyclone. *J. Meteor. Soc. Japan,* **60,** 369–379.

Rotunno, R., 1981: On the evolution of thunderstorm rotation. *Mon. Wea. Rev.*, **109,** 577–586.

——, J. B. Klemp, and M. L. Weisman, 1988: A theory for strong, long-lived squall lines. *J. Atmos. Sci.*, **45,** 463–485.

Rutledge, S. A., R. A. Houze, Jr., M. I. Biggerstaff, and T. Matejka, 1988: The Oklahoma–Kansas mesoscale convective system of 10–11 June 1985: Precipitation structure and single-Doppler radar analysis. *Mon. Wea. Rev.*, **116,** 1409–1430.

Smull, B. F., and R. A. Houze, Jr., 1985: A midlatitude squall line with a trailing region of stratiform rain: Radar and satellite observations. *Mon. Wea. Rev.*, **113,** 117–133.

Stirling, J., and R. M. Wakimoto, 1989: Mesoscale vortices in the stratiform region of a decaying midlatitude squall line. *Mon. Wea. Rev.*, **117,** 452–458.

Stensrud, D. J., R. A. Maddox, and C. L. Ziegler, 1991: A sublimation-initiated mesoscale downdraft and its relation to the wind field below a precipitating anvil cloud. *Mon. Wea. Rev.*, **119,** 2124–2139.

Velasco, I., and J. M. Fritsch, 1987: Mesoscale convective complexes in the Americas. *J. Geophys. Res.*, **92,** 9591–9613.

Verlinde, I., and W. R. Cotton, 1990: Mesoscale vortex-couplet observed in the trailing anvil of a multi-cellular convective complex. *Mon. Wea. Rev.*, **118,** 993–1010.

Wang, B., and I. Orlanski, 1987: Study of a heavy rain vortex formed over the eastern flank of the Tibetan plateau. *Mon. Wea. Rev.*, **115,** 1370–1393.

Wetzel, P. J., W. R. Cotton, and R. L. McAnelly, 1983: A long-lived mesoscale convective complex. Part II: Morphology of the mature complex. *Mon. Wea. Rev.*, **111,** 1919–1937.

Wilhelmson, R. B., and J. B. Klemp, 1978: A three-dimensional numerical simulation of splitting that leads to long-lived storms. *J. Atmos. Sci.*, **35,** 1037–1063.

Wu, G.-X., and S.-J. Chen, 1985: The effect of mechanical forcing on the formation of a mesoscale vortex. *Quart. J. Roy. Meteor. Soc.*, **111,** 1049–1070.

Zhang, D.-L., 1989: The effect of parameterized ice microphysics on the simulation of vortex circulation with a mesoscale hydrostatic model. *Tellus,* **41A,** 132–147.

——, and J. M. Fritsch, 1986: Numerical simulation of the meso-β scale structure and evolution of the 1977 Johnstown flood. Part I: Model description and verification. *J. Atmos. Sci.*, **43,** 1913–1943.

——, and ——, 1987: Numerical simulation of the meso-β scale structure and evolution of the 1977 Johnstown flood. Part II: Inertially stable warm-core vortex and the mesoscale convective complex. *J. Atmos. Sci.*, **44,** 2593–2612.

——, and ——, 1988a: Numerical sensitivity experiments of varying model physics on the structure, evolution and dynamics of two mesoscale convective systems. *J. Atmos. Sci.*, **45,** 261–293.

——, and ——, 1988b: A numerical investigation of a convectively generated, inertially stable, extratropical warm-core mesovortex over land. Part I: Structure and evolution. *Mon. Wea. Rev.*, **116,** 2660–2687.

——, and K. Gao, 1989: Numerical simulation of an intense squall line during 10–11 June 1985 PRE-STORM. Part II: Rear inflow, surface pressure perturbations and stratiform precipitation. *Mon. Wea. Rev.*, **117,** 2067–2094.

——, and Cho, 1992: The development of negative moist potential vorticity in the stratiform region of a simulated squall line. *Mon. Wea. Rev.*, **120,** 1322–1341.

——, K. Gao, and D. B. Parsons, 1989: Numerical simulation of an intense squall line during 10–11 June 1985 PRE-STORM. Part I: Model verification. *Mon. Wea. Rev.*, **117,** 960–994.

Zipser, E. J., 1969: The role of organized unsaturated convective downdrafts in the structure and rapid decay of an equatorial disturbance. *J. Appl. Meteor.*, **8,** 799–814.

——, 1977: Mesoscale and convective-scale downdrafts as distinct components of squall-line structure. *Mon. Wea. Rev.*, **105,** 1568–1589.